CHALMERS

Design of an Experimental Facility for Investigating the Flow in a Low Pressure Turbine Exit Structure

BORJA ROJO

Department of Applied Mechanics
CHALMERS UNIVERSITY OF TECHNOLOGY
Göteborg, Sweden 2015

THESIS FOR THE DEGREE OF LICENTIATE OF ENGINEERING IN THERMO AND FLUID DYNAMICS

Design of an Experimental Facility for Investigating the Flow in a Low Pressure Turbine Exit Structure

BORJA ROJO

Department of Applied Mechanics
CHALMERS UNIVERSITY OF TECHNOLOGY

Göteborg, Sweden 2015

Design of an Experimental Facility for Investigating the Flow in a Low Pressure Turbine Exit Structure
BORJA ROJO

Thesis for the degree of Licentiate of Engineering 2015:20
ISSN 1652-8565
Department of Applied Mechanics
Chalmers University of Technology
SE-412 96 Göteborg
Sweden
Telephone: +46 (0)31-772 1000

Chalmers Reproservice
Göteborg, Sweden 2015

Design of an Experimental Facility for Investigating the Flow in a Low Pressure Turbine Exit Structure
Thesis for the degree of Licentiate of Engineering in Thermo and Fluid Dynamics
BORJA ROJO
Department of Applied Mechanics
Chalmers University of Technology

Abstract

This report presents the design of a turbine facility for investigating the flow in the EES located at Chalmers University of Technology. The EES is the structure located downstream of the LPT in a jet engine. In this rig, in order to generate realistic inlet boundary conditions for the EES, an LPT stage is located upstream of the EES. The facility is a large-scale low-speed annular cascade, and the flow Reynolds number based on the channel height in the turbine stage is 465,000, which is representative for large turbofan engines. The design of the facility follows classical low-speed wind tunnel design. Experimental correlations obtained from data collected in a previous rig and from previous studies in low-speed wind tunnels were used to compute pressure losses. CFD tools have been used in the design of the facility. A short description of FEA performed in the LPT rotor and structure is included.

Keywords: Aerodynamics, Gas Turbine, Outlet Guide Vane, Exit Guide Vane, Engine Exit Structure, Turbine Exhaust Case, Turbine Rear Frame, Turbine Rear Structure, Wind Tunnel, Experimental, CFD, Heat transfer.

List of publications

This thesis is based on the work contained in the following publication:

1 B. Rojo, D. Kristmundsson, V. Chernoray, C. Arroyo, and J. Larsson, "Facility for investigating the flow in a low pressure turbine exit structure," in *11th European Conference on Turbomachinery Fluid Dynamics and Thermodynamics, ETC 2015*, 2015

Other publications which are basis for future studies in the LPT-OGV facility:

2 B. Rojo, V. Chernoray, M. Johansson, and M. Golubev "Experimental heat transfer study in an intermediate turbine duct," in *49th AIAA/ASME/SAE/ASEE Joint Propulsion Conference*, 2013

3 B. Rojo, C. Jimenez, and V. Chernoray, "Experimental heat transfer study of endwall in a linear cascade with IR thermography," in *EPJ Web of Conferences*, vol. 67, p. 02100, EDP Sciences, 2014

4 M. Bovo, B. Rojo, and M. Golubev, "Measurements of a single pulse impinging jet. A cfd reference," in *EPJ Web of Conferences*, vol. 67, p. 02010, EDP Sciences, 2014

5 M. Bovo and B. Rojo, "Single pulse jet impingement on inclined surface, heat transfer and flow field," tech. rep., SAE Technical Paper, 2013.

Acknowledgements

First, I would like to thank my supervisor, Valery Chernoray, for giving me the opportunity to work in this exciting project. His support during these years was essential to perform the work showed in this thesis.

Thereafter, much credit goes to my co-supervisor at GKN Aerospace Sweden, Carlos Arroyo, whose advices were of incalculable value for me. His perseverance and hard work are worthy of admiration and gratitude.

Special thanks to Jonas Larsson for all his support during this time. All the inspiring discussions and help were source of great ideas for the project. I will always be grateful for his advises.

During my work at Chalmers, Fredric Carlsvärd, Darri Kristmundsson and Carlos Jimenez Sanchez (We) helped me with the design of the rig and to enjoy life outside my office walls. You made easier to stand the dark, cold and unforgiving Swedish winter. Thanks to Mirko Bovo for the great time that 'We' spent in the lab and for your friendship. I would also like to thank Martin Johansson for all the discussions we had in his office and his clever advices. In addition, I would like to thanks all my colleges at the fluid dynamics division who made more enjoyable the time in the office. I will always remember the unpredictability of the discussion topics during fika.

Thanks to Monica Marcos for teaching me the value of friendship no matter the circumstances.

Last but not least important, I would like to thank my family for being always there to support me no matter what. Without them, I would not manage to achieve most of my goals. Gracias!

This work was funded by the Turbokraft research program. This project was carried out at the Department of Applied Mechanics, Division of Fluid Dynamics at Chalmers University of Technology, in co-operation with GKN Aerospace Sweden.

There is a driving force more powerful than steam, electricity and atomic energy: the will.
- Albert Einstein

Nomenclature

Acronyms

CFD	Computational Fluid Dynamics.
EES	Engine Exit Structure.
EGV	Exit Guide Vane.
FEA	Finite Element Analysis.
HPT	High Pressure Turbine.
IR	Infrared.
ITD	Intermediate Turbine Duct.
LPT	Low Pressure Turbine.
NACA	National Advisory Committee for Aeronautics.
NGV	Nozzle Guide Vane.
OGV	Outlet Guide Vane.
SST	Shear Stress Transport.
TEC	Turbine Exhaust Case.
TRF	Turbine Rear Frame.
TRS	Turbine Rear Structure.

Latin

A	Amplitude of the acceleration function $[m/s^2]$.
K	Pressure loss coefficient.
L	Length of the contraction duct $[m]$.
P_T	Total pressure $[Pa]$.
P	Static pressure $[Pa]$.
Re	Reynolds number.
R	Radial distance $[m]$.
S	Cross-section area $[m^2]$.
$\dot{m}$	Mass flow rate $[kg/s]$.
a	Acceleration of the fluid $[m/s^2]$.

c	Distance from contraction inlet to beginning of damping function [m].
d	Distance from contraction inlet to end of damping function [m].
k	Turbulent kinetic energy [m^2/s^2].
p	Distance from contraction inlet to nose cone [m].
s	Parameter to define the central body.
u_0	Axial velocity at the contraction inlet [m/s].
u	Axial velocity [m/s].
x	Axial distance [m].
y^+	Dimensionless wall distance.

Greek symbols

β	Open area ratio [%].
ϵ	Turbulent dissipation rate [m^2/s^3].
κ	Parameter for acceleration function.
λ	Parameter for acceleration function.
ω	Specific dissipation rate [$1/s^1$].
ρ	Air density at standard conditions [kg/m^3].

Subscripts

1	Inlet.
2	Outlet.
cb	Relative to central body.
c	Relative to contraction section.
d	Relative to contraction duct.

Contents

Abstract **i**

List of publications **iii**

Acknowledgements **v**

Nomenclature **ix**

1 Introduction **1**
1.1 Description of the work 2
1.2 Aims 3

2 Experimental Facility **5**
2.1 General description of the facility 5
2.2 Requirements for the facility 5
2.3 Components 7
2.3.1 Fan 7
2.3.2 Diffusing section 8
2.3.2.1 Corner design 8
2.3.2.2 Diffusers design 8
2.3.2.3 CFD analysis of the diffusing section 9
2.3.3 Flow conditioning section 12
2.3.4 Contraction section 13
2.3.4.1 Aero design 13
2.3.4.2 Volume flow meter 16
2.3.5 Turbine section 18
2.3.5.1 Struts and annular screen 18
2.3.5.2 Braking system 20
2.3.5.3 Turbine stage 21
2.3.5.4 Aero design of the turbine stage 21
2.3.5.5 Mechanical design of the turbine stage 23
2.3.6 Engine exit structure 27
2.4 Pressure drop calculation 28

3 Conclusions **31**

3.1 Future work 31

4 My Contributions **33**
4.1 Paper 1 33
4.2 Additional work 33

Bibliography **35**

1 Introduction

Demands from industry to improve the efficiency of energy systems, including aero engines, are leading to research focused on more efficient propulsion systems. Energy efficiency can be increased in jet engines by increasing the by-pass ratio or introducing geared engines. As a consequence, LPT OGV[1] inlet swirl angles are increased for ungeared two-spool engines or geared engines that have increased off-design swirl variations. Therefore, LPT OGV aerodesign is becoming more demanding and new experimental data on OGV designs are required.

OGVs are located downstream of the last stage of the LPT in an aero engine, as shown in Fig. 1.0.1. The main structural purpose of this component is to connect the rear engine mounts with the low-pressure axis bearing. The OGVs thus carry the loads from the engine. Furthermore, OGVs should provide space for oil tubes, oil scavenge tubes and electrical cables passing from the outer case to the shaft of the engine. In addition to the structural and connective functions, the OGVs also play an important aerodynamic role in an aero engine because they remove the swirl that comes from the LPT situated upstream.

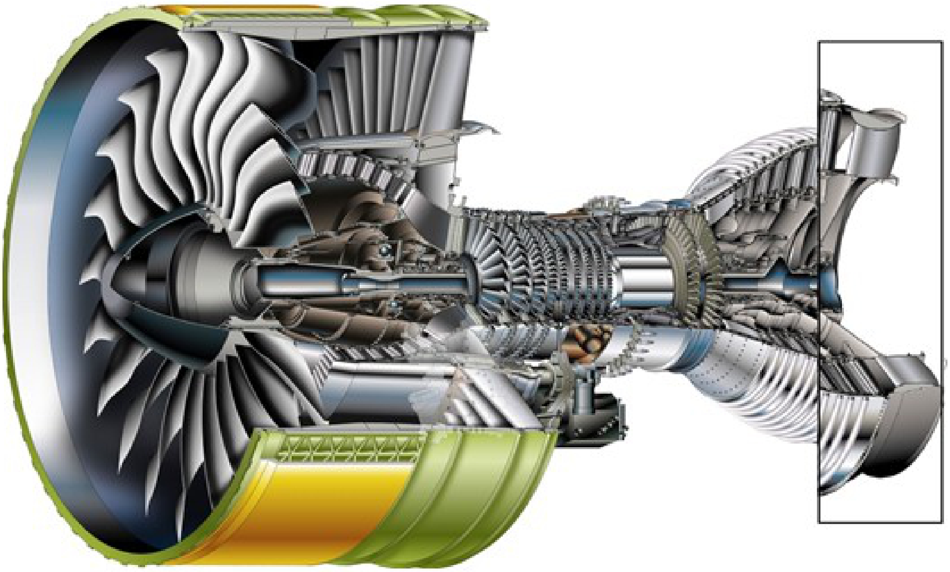

Figure 1.0.1: *GP7000 turbofan engine, from [1].*

The flow around an OGV is inherently complex, involving wakes from the upstream turbine (see Goldstein and Spores [2]), interaction of boundary layers and the risk of flow separation. Due to the small number of OGVs in the EES[2] (typically 12), it is very

[1]Also known as EGV.
[2]Also known as TEC, TRF or TRS.

important to study secondary flow. Structural requirements on the EES lead to the use of polygonal endwalls and sunken engine mounts that furthermore complicate the aerodesign in the shroud region. The design parameters that are required from an aerodynamic point of view are minimization of the pressure drop and the capability to withstand flow separation. Moreover, the prediction of flow separation and heat transfer becomes more crucial when the OGV has an inlet incidence angle different from the on-design operation condition. Modern geared engines show large swirl angle variations and high temperatures at off design conditions; hence, heat transfer predictions become critical and relevant validations from this type of rig are needed.

Although experimental data of the flow in the EES and outlet guide vanes exist, these are insufficient for CFD validation. Most of the experimental data available for flow around OGVs are either representative of old OGV designs or have been from experiments in linear cascades (see Hjärne et al. [3], Hjärne [4] and Rojo et al. [5]), which are valuable for 2D validations. Recently, Schönleitner et al. [6] showed that an annular cascade rig with an LPT upstream of the test section can provide realistic data on the complex flow inside the EES. In addition, it is of great interest to study large variations from on-design conditions at the inlet of the OGVs, as OGVs should be able to withstand these variations inside an aero engine.

Finally, it is important to point out that, even though current LPTs operate close to sonic conditions, most of the physical phenomena involved in the EES section are also present at low speed, such as secondary flows, rotating wakes and interaction with the duct endwalls. Hence, the experimental data obtained from this annular cascade rig can be valuable for CFD validation and component testing. Furthermore, building a high-speed rig would have become expensive and would have been difficult to operate, and very high requirements would have been imposed on the measurement techniques.

1.1 Description of the work

This report presents the work done at Chalmers University of Technology. Most of the work presented in this thesis is numerical, other than static pressure measurements in an existing rig located at this institution.

The main focus here is on explaining all the aerodesign work as part of the design work and includes a small portion of FEA carried out for safety and deformation prediction purposes. Regarding aerodesign, GKN Aerospace Sweden provided the aero surfaces of the turbine and EES that will be tested in this facility. The rest of the components have been designed at Chalmers University of Technology.

At the beginning of the project, an upgrade of the existing facility (see Arroyo [7]) was thought to be sufficient to provide a realistic Reynolds number in the test section. Then, after several design iterations, the construction of a larger facility was found necessary to achieve realistic engine Reynolds numbers in the test section. Hence, all components of this new facility needed to be designed. For the design of the facility, CFD tools were used to analyze most of the components inside the facility. The goals of these studies were to obtain the required flow quality in each section and to optimize the length of some components.

A thermal design of the facility and hydraulic system to connect the different components was also done.

1.2 Aims

This research aims to investigate the highly complex flows from an LPT to an EES and their influence on aero performance and heat transfer. This will lead to a better understanding of the phenomena involved in this section of the engine and provide validation data for CFD.

The pressure losses inside the EES is of great interest for validation of the tools used for the design of the EES. In addition, it is very important to study secondary flows because a low aspect ratio in the EES designs is more sensitive to changes in the inlet flow. Predicting flow separation is of great interest as well because of the complexity of the flow inside this section. Studying these phenomena at on-design and off-design conditions will lead to the development of more robust aero designs. It is complex to predict transition phenomena, and they have a great influence on the flow structures and heat transfer over the OGVs.

The flow around realistic engine mounts inside the EES is highly 3D and difficult to predict. Another realistic feature of this engines that it is interesting to study is the interaction of the P-flange pocket with the tip flow leakage and the outlet flow from the LPT. In addition, other realistic features inside the EES such as welds and milling cusps will be studied in this rig.

In sum, the main purpose of designing and building this facility is to study the interaction of all the physical phenomena mentioned above. At the same time, experimental techniques will be developed in this project at Chalmers University of Technology that focus on IR thermography techniques.

2 Experimental Facility

2.1 General description of the facility

The rig is set to be a closed loop facility where an LPT is located upstream of the test section in order to provide engine realistic inlet boundary conditions to the EES. There is a return channel downstream of the EES that connects the flow outlet from the test section to a centrifugal fan. Figure 2.1.1 shows the rig layout. There is a centrifugal blower that is driven by an electrical motor. A straight duct is located downstream of the fan outlet to obtain better flow with minimal losses in the rest of the facility and less noise generation (especially in the diffusing section). Afterwards, there is a vaned corner duct and a diffuser duct (see 2.3.2.1 and 2.3.2.2). The diffusing angle was selected to be as low as possible to reduce the risk of large flow separation and unsteadiness. There is a second diffuser duct after the second vaned corner to obtain a 2x2 meters square cross section.

The flow is cooled after the diffusers to approximately $30°C$ in a heat exchanger. It is important to control the flow temperature since one of the requirements for this facility is a steady flow with good repeatability. Heat transfer experiments will be performed in the future, and this makes having a controlled steady temperature crucial. Furthermore, the heat exchanger produces the second highest pressure loss in the rig and this will be helpful in increasing flow uniformity and reducing the losses in the settling chamber located downstream of this section. Most low-speed wind tunnels situate the heat exchanger upstream of the flow conditioning section (see Bradshaw and Pankhurst [8]).

A honeycomb and 5 screens are located in the settling chamber to improve the flow uniformity. The honeycomb is used to remove swirl flow and cross velocity fluctuations. Turbulence screens are used to make the flow uniform. The contraction duct with the central body is located downstream of this section. After this contraction, an annular straight section drives teh flow from the contraction section to the LPT stage. There are two rows of four NACA 0015 struts and a turbulence screen in between to remove the wakes generated by these struts. The LPT stage has 60 NGVs at the stator and 72 blades at the rotor. The rotor blades are shrouded, and the tip flow leakage is representative of aero engines in terms of mass the flow ratio between the main flow and the leakage flow. To control the rotational speed of the turbine, a hydraulic pump is connected to the rotor's shaft. Afterwards, the flow passes through the EES, where most of the measurements will take place. Purge flow coming from the rotor cavity and pass through the rim seal will be included and will interact with the main flow. Although the EES is the main component that will be studied, it has an additional function in this facility, which is to straighten the flow coming from the LPT. The outlet flow coming from EES should therefore be fully axial. Finally, the flow at the outlet of this section will return to the fan inlet.

2.2 Requirements for the facility

The main requirements of this facility are listed below.

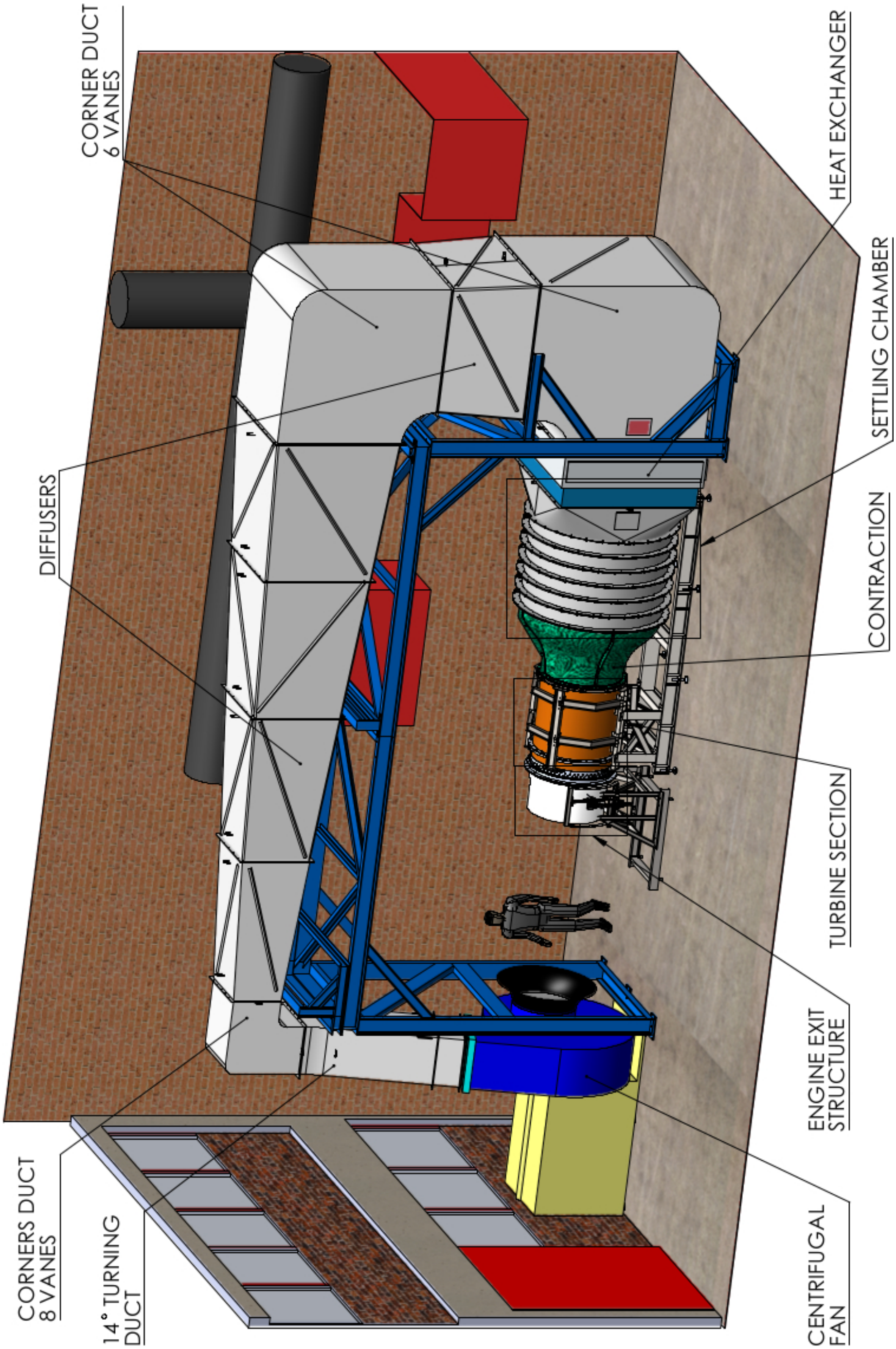

Figure 2.1.1: *Rig layout.*

- **Reynolds number similarity.** It is important to have a Reynolds number at the inlet of the turbine stage and EES section that is similar to what can be found in a real aero engine in order to achieve flow characteristics comparable with a real engine. In this facility, the Reynolds number is about 350,000 based on the axial chord of the OGVs. For large ungeared engines, the Reynolds number can be around 450,000 and, for a smaller engine such as a geared turbofan engine, the Reynolds number can be over 300,000.

- **Stable operating conditions and repeatability.** In this experimental rig, a steady flow (velocity, pressure and temperature) is needed into the turbine stage and EES. Furthermore, the same results should be obtained under the same conditions in this facility.

- **Representative inlet flow to the EES.** It is required that the flow from the turbine has representative wakes and secondary flows, swirl and mass flow distributions, tip leakage flow and rim-seal purge flow. It should be possible to cover important off-design variations (from -25° to -45°) and to vary swirl angles, mass flow and Re numbers.

- **Access for the measurement techniques.** Access and traversing systems for the different measurement techniques should be provided, while the disturbances to the flow should be kept to a minimum.

- **Modular design.** A modular design will enable the possibility of exchanging the EES and testing different configurations.

- **CFD friendly.** To decrease the computational resources needed for CFD simulations, the ratio between the number of NGVs and/or rotor blades and OGVs should be a low integer number (in our case 60/72/12).

2.3 Components

This section explains the function and design criteria of all the components used in this experimental facility.

2.3.1 Fan

The centrifugal fan was selected to provide the required flow rate and pressure. Classical low-speed wind tunnels use an axial fan because it can provide a higher mass flow than a centrifugal blower but a lower pressure ratio. Due to the high pressure drop required to run the turbine, a centrifugal blower was selected. A frequency converter drives the motor and allows for a continuous regulation of the mass flow rate in the facility. Elastic connections are used between the fan and the rest of the facility in order to avoid propagating the vibrations of the fan to the neighboring components. Table 2.3.1 shows the main characteristics of the fan unit.

Parameter	**Value**
Design volume flow rate [m^3/h]	6900
Design total pressure [kPa]	7.56
Fan wheel diameter [mm]	1620
Maximum rotational speed [rpm]	1800
Electric motor maximum power [kW]	200
Total efficiency	0.82
Noise levels [dB]	114.1

Table 2.3.1: Fan main characteristics.

A straight duct is located downstream of the elastic connector. The purpose of having this duct is to obtain a more uniform flow into the diffusing section and, therefore, lower aero losses and noise.

2.3.2 Diffusing section

Due to the fact that the pressure losses in the heat exchanger and flow conditioning are proportional to the velocity square and function of the Reynolds number, the air flow coming out from the centrifugal fan outlet (a rectangular section of 710x900 mm) must be diffused to a larger cross section area (a square section of 2,000x2,000 mm) in order to reduce the pressure required to drive the given flow through the facility. The most important requirements for this section are to provide the area change and turn the flow with minimum losses, flow separation and non-uniformities.

2.3.2.1 Corner design

All the corners have been designed according to the guidelines found in Barlow et al. [9]. These corners are equipped with guide vanes, which are bent plates with a straight trailing edge. Thick, solid vanes generate more uniform flow, but constant thickness vanes made of thin plates are more economical and can deliver the required performance.

Due to the high Reynolds number at the inlet of these components (over 500,000), the gap-chord ratio chosen for the guide vane design is 1:4 (see Barlow et al. [9]). The first corner contains eight vanes and the second contains six vanes. The third corner is a scaled up design of the second corner.

CFD analysis was made to verify the aero design of this component and showed good agreement with empirical data.

2.3.2.2 Diffusers design

In classical low-speed wind tunnel design, the diffuser is one of the most important components. A bad diffuser design can lead to high losses, noise generation and non uniform flow even if there is a settling chamber. Therefore, this component has been designed with the smallest diffuser angle possible (there is space limitation in the facility). Both of the diffuser ducts have the same diffuser half angle of 3.75°.

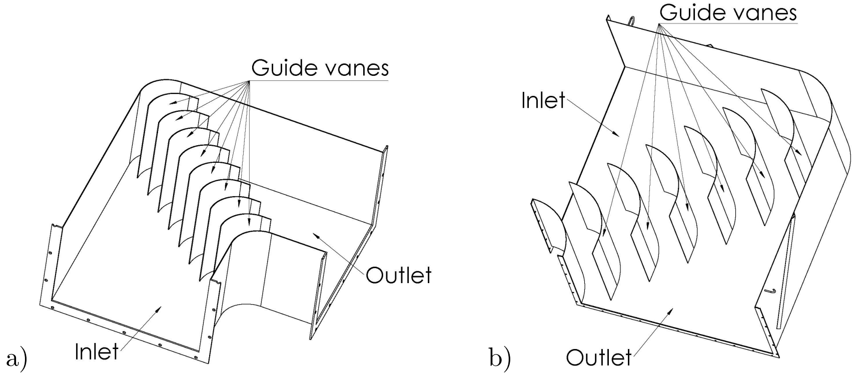

Figure 2.3.1: *a) Section view of the first vaned corner b) Section view of the second and third vaned corner.*

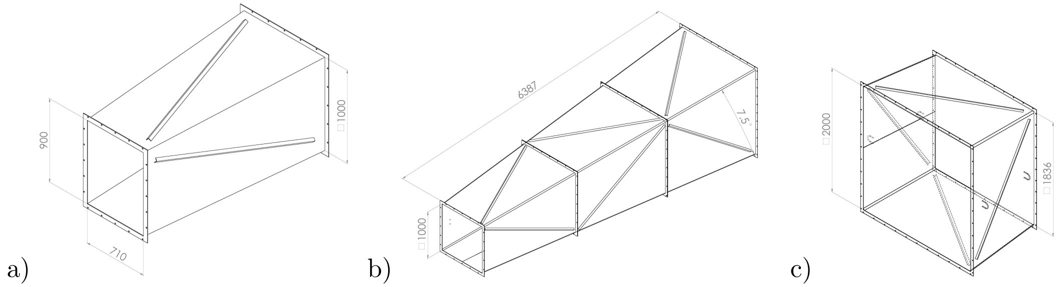

Figure 2.3.2: *a) Rectangular to square section diffuser duct b) First square diffuser duct c) Second square diffuser duct between second and third corner*

The fact that the flow velocity profile at the outlet of the centrifugal fan is unknown and not uniform might increase the losses in the diffusing section and cause flow non-uniformity. For this reason, the possibility of adding a turbulence screen inside the first square diffuser was provided. This is explained in detail in section 2.3.2.3.

2.3.2.3 CFD analysis of the diffusing section

By means of CFD analysis, different configurations were evaluated for the design of the diffusing section. First, a 2D steady state study was performed in order to obtain an approximate value for the pressure losses and velocity distribution. In this study, a uniform velocity was set as the inlet boundary condition and outflow at the outlet of the diffusing section. A constant pressure drop coefficient was set in the heat exchanger, which is calculated from data given by the manufacturer of this component. The numerical grids were generated in ICEM ANSYS, and FLUENT was used as a solver. Figure 2.3.3 shows the effect of locating guide vanes inside the corners. The pressure losses are reduced 11%, and there are no recirculation areas where aeroacoustic noise is generated.

Furthermore, $k-\omega$ SST and $k-\epsilon$ turbulence models were compared, obtaining similar

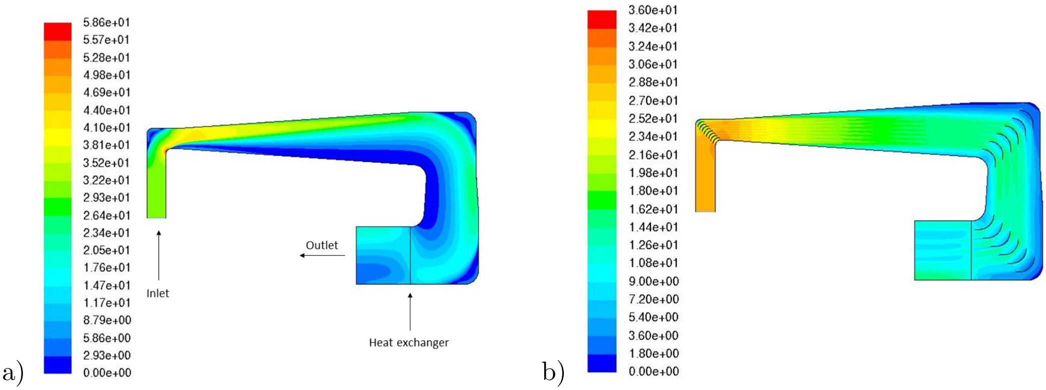

Figure 2.3.3: *a) Velocity field from 2D CFD simulation without guide vanes in the corner ducts b) Velocity field adding guide vanes. Both simulations are performed using the $k-\omega$ SST turbulence model with $y^+ < 1$.*

pressure losses (less than 0.1% difference). The $k-\epsilon$ model shows a slightly more uniform velocity distribution at the outlet, but not significant enough to consider further studies on the selection of a turbulence model.

The vaned 2D case was analyzed with two different meshes. The main purpose was to check the dependency of the result on the use of wall functions ($40 < y^+ < 100$) or having resolved boundary layers ($y^+ < 1$). Both cases were studied using the $k-\omega$ SST model. The outcome of this study showed that the difference between these two cases in terms of pressure losses is a 0.25% higher pressure loss using wall functions. Regarding the velocity distribution, there are no differences between these cases. Hence, wall functions can be used in the 3D case since it is computationally less expensive. Figure 2.3.4 shows the numerical mesh for the 3D case. The mesh contains 6.7M cells and it is structured.

The main goals of this CFD simulation are to obtain the pressure losses with a realistic geometry, the influence of having a 14° turning downstream of the fan outlet on the diffuser performance and the effect of a corner vortex, which the 2D CFD cannot predict, on the pressure losses. In addition, the effects of locating a turbulence grid inside the long diffuser duct is studied and a suitable location in case it is needed. For this study, the $k-\omega$ SST turbulence model was used. Uniform velocity inlet boundary conditions were used and outflow at the outlet.

Figure 2.3.5 shows a comparison between the case without grids and the position selected for the location of a turbulence grid. To select the suitable location for the screen, three locations (first, second and third) and different pressure drops for each screen were checked.

First of all, a large separation in the top-left corner of the long diffuser duct can be observed in Fig. 2.3.5 a). This flow structure is much larger than in the other three corners of the diffuser duct for two different reasons. First, looking at Fig. 2.3.3, the velocity is not symmetric with respect to the centerline of the first diffuser duct due to overturning the flow in the first corner. This could be fixed by having a slightly larger angle between the leading and the trailing edges of the vanes. In addition, the area

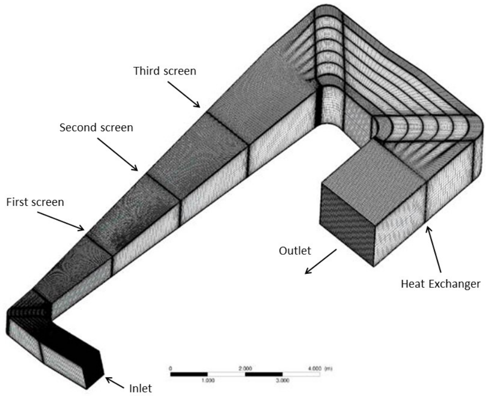

Figure 2.3.4: *Computational mesh for the full diffusing section*

where the velocity starts to become non-symmetric in Fig. 2.3.3 b) is the same as for the corner separation. Second, the lack of guide vanes inside the 14° turning duct leads to a non-uniform velocity distribution at the outlet of the first corner duct and, therefore, a larger separation on the top-left corner and a larger corner vortex on the top-right corner of the diffuser.

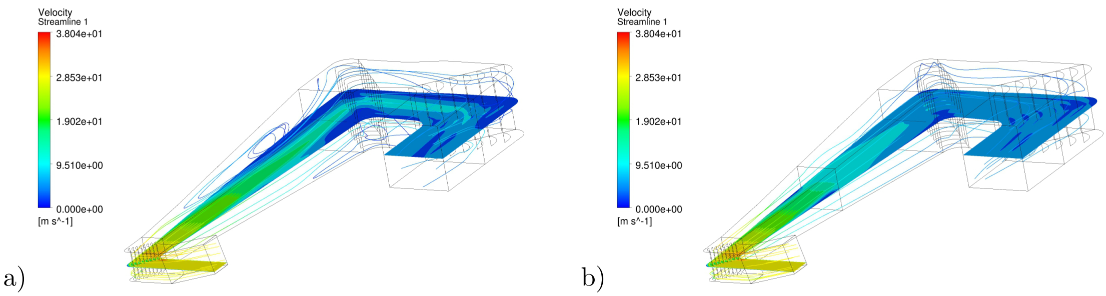

Figure 2.3.5: *a) Velocity distribution inside the diffusing section without turbulence grids b) Velocity distribution with a turbulence grid located in the middle of the long diffuser duct.*

On the other hand, a turbulence grid could remove the large corner recirculation, giving a more uniform profile at the outlet of the heat exchanger. In addition, guide vanes have been added to the 14° turning duct in order to avoid having such a large corner separation. It is important to point out that these CFD simulations are performed under the assumption of a uniform flow inlet, which is not the case. There are no data available from the manufacturer regarding flow or pressure distribution at the outlet of the fan. In any case, even if there are large flow structures or a non-uniform velocity distribution from the centrifugal fan, having a heat exchanger and adding a turbulence screen will lead to a satisfactory flow quality coming into the flow conditioning section.

2.3.3 Flow conditioning section

The flow from the heat exchanger has a non-uniform distribution. There are several sources of non uniformities in the existing facility. First, the centrifugal fan generates wakes and secondary flows that might not be dissipated through the diffusing section. Moreover, the guide vanes located in the corners and the 14° turning duct also generate wakes, which can be seen in Fig. 2.3.3 and 2.3.5. Furthermore, due to geometric tolerances and the manufacturing process, there is no guarantee that all the guide vanes are in the correct position, and flow non uniformities are created in the diffusing section. In addition, the flow can be affected by the negative pressure gradient inside the diffuser ducts, generating areas with high velocities and low velocities or, in some cases, flow separation. The approach taken to solve this problem is to use honeycombs to reduce the transversal velocity components and a set of turbulence screens to obtain higher flow uniformity. The arrangement of these components is shown in Fig. 2.3.6.

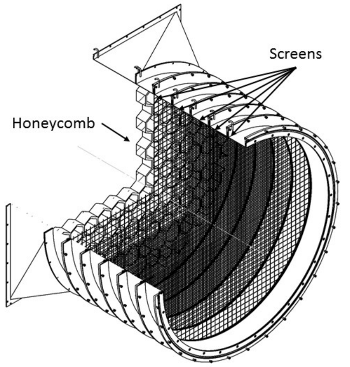

Figure 2.3.6: *Computational mesh for the full diffusing section*

The flow should go through a contraction duct to change the square cross section (2x2 meters) coming from the heat exchanger to a circular section with a diameter of two meters. To minimize the length of the square to circular section duct, CFD was performed to check whether corner wakes generated in this duct could be removed. The length chosen for this duct after numerical analysis is 500 mm.

The air flow then passes through a honeycomb. The honeycomb is used in low-speed wind tunnels as a guiding device through which air filaments are rendered parallel (definition given by Prandtl). A non-uniform axial velocity distribution can be expected downstream of the honeycomb. The honeycomb chosen has hexagonal cells with a length of 110 mm, a hydraulic diameter of 14 mm and a length-to-cell diameter of 8. These values are as recommended in Barlow et al. [9] and Mehta and Bradshaw [10].

Finally, the air flow passes through 5 turbulence screens to reduce flow non-uniformities in the axial direction and turbulence intensity. According to Barlow et al. [9], the best result can be obtained with several screens with a coarser to finer mesh size and wire diameter, each a turbulence screen with an equivalent pressure drop coefficient. Groth and Johansson [11] suggest starting with a relatively coarse grid followed by a finer one.

Table 2.3.2 summarizes the main screen parameters.

Screen number	**1**	**2**	**3**	**4**	**5**
Cell width [mm]	4	2.5	1.75	1.25	1
Wire diam. [mm]	1	0.7	0.5	0.33	0.24
β [%]	64	61	60	63	65
Wire Re	387	271	194	128	93
K	0.75	1.01	1.13	1.1	1.01

Table 2.3.2: Main screen parameters. Pressure loss coefficient (K) calculated according to Barlow et al. [9].

The screens were selected based on a similar existing flow conditioning section of a facility located at Chalmers University of Technology (see Arroyo et al. [12])

2.3.4 Contraction section

The contraction connects the outlet of the flow conditioning section with the straight annular section of the turbine. This is done by placing a central body in front of the hub pipe and a contraction duct with a length of 1 meter. Another use of this contraction is to measure the mass flow inside the facility by means of the pressure at the inlet and outlet. This application of the contraction is widely used in wind tunnels and is similar to a Venturi meter. The main requirements that the contraction must fulfill are listed below.

- **Minimum contraction length.** It is critical to design a short contraction so that there is enough space to place the turbine section and EES in the facility. Therefore, the first parameter that is taken into account is the length of the contraction. In this case, a 1 m length contraction was achieved with an area ratio of 4.7 and a length to inlet diameter ratio of 0.5.

- **Flow quality.** Generally, contractions are not sources of high pressure drops and, furthermore, the flow quality (from a wind tunnel perspective) can be increased if the contraction is correctly designed. Hence, once the contraction has been designed, CFD techniques are used to check that the flow quality at the outlet is good enough for our purposes.

2.3.4.1 Aero design

In an extensive literature search of this kind of contraction, no reports or examples of contraction design with a central body criteria were found (see Morel [13], Mikhail [14], Abbaspour and Shojae[15], Bell and Mehta [16], Chmielewski [17]). For the geometry calculation, the air flow is assumed incompressible, inviscid, irrotational and axisymmetric. Furthermore, only the mean axial speed and acceleration of the fluid are analyzed (1D problem).

$$a(x) = u\frac{\partial u}{\partial x} \tag{2.3.1}$$

Using all the assumptions listed above, the expression for the flow acceleration becomes as shown in Eq. 1. This could lead to an analytic solution in simple cases, i.e. axisymmetric contraction design without a central body based on a continuous acceleration function (see Chmielewski, [17]). Unfortunately, the central body produces a discontinuity in the acceleration function.

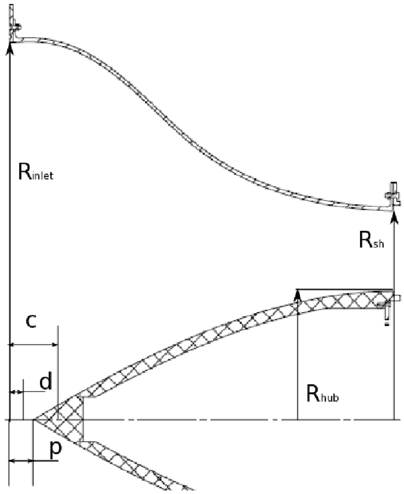

Figure 2.3.7: *Cross-section of the contraction.*

Furthermore, the acceleration function that provides the best shape for the duct and central body is not known. The following acceleration function has been used which is similar to the function used by Chmielewski [17] for a contraction without central body.

$$a(x) = A \cdot f(x) = A \cdot \left[\sin\left(\frac{\pi x}{L}\right)^{\kappa}\right]^{\lambda} \tag{2.3.2}$$

Here $x \in [0, L]$ and $f(x) \geq 0$ for all x inside this interval. κ and λ are parameters and A is a constant. Now, the next step is to calculate the value of the constant A (or amplitude of the function). In order to calculate this value, it is necessary to integrate eq.2.3.1.

$$\int_0^x a(x) = \int_0^x u\frac{\partial u}{\partial x} \Rightarrow \int_0^x a(x)dx = \int_0^x udu \Rightarrow \frac{u(x)^2 - u_0{}^2}{2} = A\int_0^x f(x)dx$$

$$u(x) = \sqrt{2A\int_0^x f(x)dx + u_0{}^2} \tag{2.3.3}$$

Equation 2.3.3 is also used later for the calculation of the velocity distribution through the contraction. The velocity at the outlet is found using the mass conservation equation.

A is calculated with Eq. 2.3.4.

$$A = \frac{u(L)^2 - {u_0}^2}{2\int_0^L f(x)dx} \tag{2.3.4}$$

Looking at Eq. 2.3.3 and 2.3.4 it can be seen that the only restriction on the definition of the function is that it must be integrable, which means that this method can be used even if $f(x)$ is not continuous. In the case of a central body, the acceleration function will be integrable but not continuous. To define the acceleration function, a set of three parameters is added: d, p and c (see fig. 2.3.7). First a constant acceleration below the ideal curve is kept so that it damps the effect of the central body on the calculation of the contraction duct. Hence, from d, the acceleration is kept constant. Parameter p shows where the nose cone should be located. Finally, c represents where the value of the acceleration without a central body and the value of the acceleration with a central body are the same. The acceleration function can thus be defined as follows:

$$f(x) = \begin{cases} \left[\sin\left(\frac{\pi x}{L}\right)^{\kappa}\right]^{\lambda} & \text{if } \; 0 \leq x \leq d \;\cup\; x \geq c \\ f(d) & \text{if } \; d < x \leq p \\ f(c) & \text{if } \; p < x < c \end{cases} \tag{2.3.5}$$

It is important to point out that, with this method, only the duct shape is calculated based on the acceleration curve. The central body is designed using a 3rd order polynomial. The boundary conditions for the polynomial are listed below.

$$B.C \; for \; R_{cb}(x) = \begin{cases} R_{cb}(x=p) = 0 \\ \left|\frac{dR_{cb}(x)}{dx}\right|_{x=p} = s \\ R_{cb}(x=L) = R_{hub} \\ \left|\frac{dR_{cb}(x)}{dx}\right|_{x=L} = 0 \end{cases} \tag{2.3.6}$$

In our case we select $s = 0.6$ and $p = 0.05$ to obtain a smooth shape that does not have an inflection point. Finally, the geometry of the duct is calculated using the mass conservation equation for incompressible flow.

$$S = \frac{\dot{m}}{\rho u} \tag{2.3.7}$$

$$R_d(x) = \begin{cases} \sqrt{\frac{\dot{m}}{\pi \rho u}} & \text{if } x \leq p \\ \sqrt{\frac{\dot{m}}{\pi \rho u} + R_{cb}(x)} & \text{if } x > p \end{cases} \tag{2.3.8}$$

A 2D axisymmetric CFD simulation was made to validate the performance of the designed contraction shape. The CFD results are shown in Fig. 2.3.8. It was concluded that the contraction fulfills all our demands in terms of flow quality (no flow separation and less than 1% flow non-uniformity at the contraction outlet) and length (1 meter long). Figure 2.3.9 shows an example of a contraction design with lower flow uniformity due to the aggressive shape of the contraction duct and the zero curvature at the end of the central body.

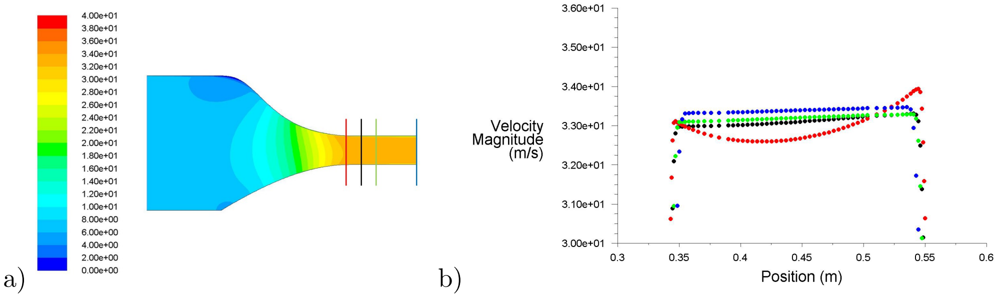

Figure 2.3.8: *a) Velocity contour plot of half a contraction section. b) Velocity profile at the exit of the contraction at different positions.*

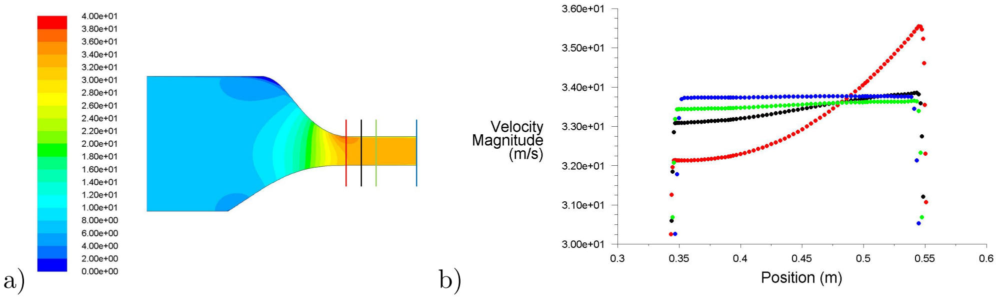

Figure 2.3.9: *a) Velocity contour plot of half a contraction section of a discarded design. b) Velocity profile at the exit of the contraction at different positions for a discarded design.*

Furthermore, the duct has been manufactured in four sectors bolted to each other with 5mm laminated glass fiber. FEA was performed and a maximum deformation lower than 0.1mm was obtained, which is negligible compared with the size of the duct. The central body has been manufactured with a glass fiber shell and a stereo foam core. Figure 2.3.10 shows images of these components.

2.3.4.2 Volume flow meter

Once the the geometry is obtained and has fulfilled the main requirements, the contraction section is ready to be calibrated (numerically) to obtain the mass flow rate inside the LPT-OGV rig.

First, the Bernoulli equation is applied between the inlet and the outlet of the contraction section, adding a pressure loss term.

$$P_1 + \frac{1}{2}\rho u_1^2 = P_2 + \frac{1}{2}\rho u_2^2 + \frac{1}{2}K_c \rho u_1^2 \tag{2.3.9}$$

Here, K_c is the pressure drop coefficient and is a function of the Reynolds number. On the other hand, applying mass conservation along the contraction Eq. 2.3.10 is obtained.

$$u_2 = u_1 \frac{A_1}{A_2} \tag{2.3.10}$$

a) b)

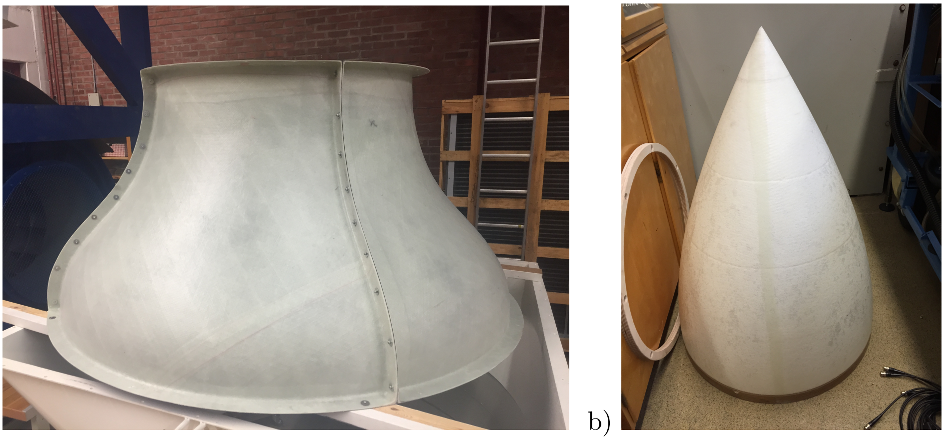

Figure 2.3.10: *a) Contraction duct b) Central body.*

Static pressures at the inlet and outlet are known since they are measured with pressure taps. Therefore, using Eq 2.3.10 in Eq. 2.3.9 and making a simplification, the following is obtained.

$$u_1 = \sqrt{\frac{2\left(P_2 - P_1\right)}{\rho} \cdot \frac{1}{1 - \left(\frac{A_1}{A_2}\right)^2 - K_c}} \tag{2.3.11}$$

From Eq. 2.3.12 it is easy to obtain the mass flow.

$$\dot{m} = \rho A_1 \sqrt{\frac{2\left(P_2 - P_1\right)}{\rho} \cdot \frac{1}{1 - \left(\frac{A_1}{A_2}\right)^2 - K_c}} \tag{2.3.12}$$

The only unknown from this equation is the pressure loss coefficient. Hence, a parametric CFD study was performed to calculate the pressure drop coefficient of the contraction section. The pressure loss coefficient calculation is obtained simplifying Eq. 2.3.9 as follows.

$$K_c = \frac{P_{T1} - P_{T2}}{\frac{1}{2}\rho u_1^2} \tag{2.3.13}$$

Here, P_T is the total pressure. The parametric study was done for mass flow values from 0.25 to 22.8 kg/s. Results of this study are shown in Fig. 2.3.11.

Figure 2.3.11 shows that the minimum value for the pressure loss coefficient (K) inside the operational range of the LPT-OGV rig is slightly higher than 0.4 for this geometry. From the point of view of pressure losses, the losses are negligible compared with the rest of the rig. On the other hand, the losses are not negligible for the calculation of the mass flow. If pressure losses are neglected, a 0.75% error would be inserted in the calculation according to the results of this analysis.

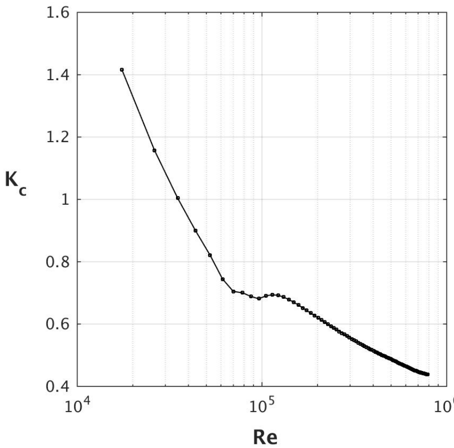

Figure 2.3.11: *Pressure loss coefficient as function of the Reynolds number for the final contraction section geometry.*

2.3.5 Turbine section

The turbine section is required to create realistic boundary conditions at the inlet of the EES. Figure 2.3.12 shows a cross section drawing of the turbine section together with the contraction and the EES.

2.3.5.1 Struts and annular screen

Downstream of the contraction section, there are two rows with four NACA 0015 profile struts. The axial chord distance of these airfoils is 300 mm and they have a maximum thickness of 45 mm. The purposes of having these components are listed below.

- Provide access from the hub interior to the exterior in order to connect oil pipes to feed the hydraulic pump. A through hole of 40 mm provides enough clearance for the pipes. Moreover, there are empty holes that could be used in the future to study the effects of purge flow coming from the hub at the inlet of the rotor.

- Connect the internal to the external structure. They are the only support between interior and exterior structures, and they are therefore, manufactured as solid steel. The struts must be stiff enough to withstand all the load without suffering large deformations. In addition, these struts should have the lowest negative impact on the flow uniformity, which is a limitation to the size of the struts. Furthermore, FEA was run on the internal structure in order to check if it can withstand the loads and for maximum deformations (see Fig. 2.3.13). The maximum displacement in this structure is lower than 0.1 mm in any direction.

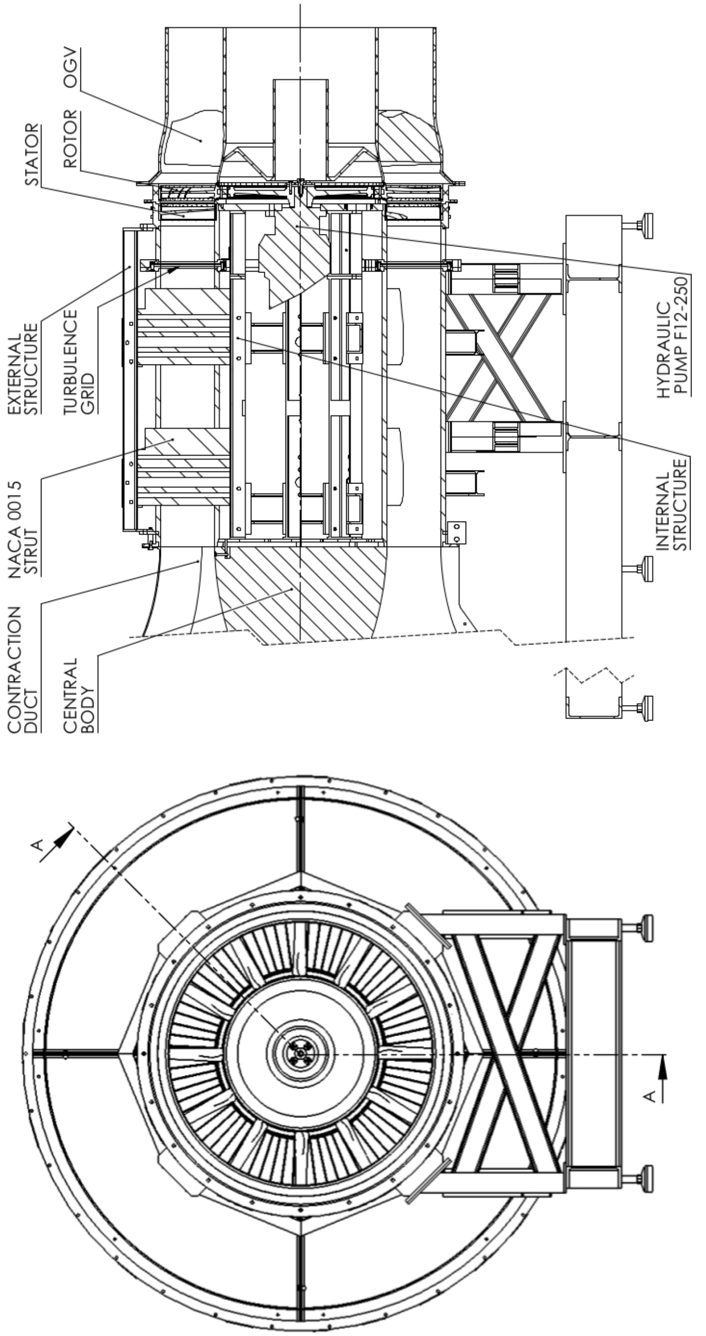

Figure 2.3.12: *Drawing of the turbine section.*

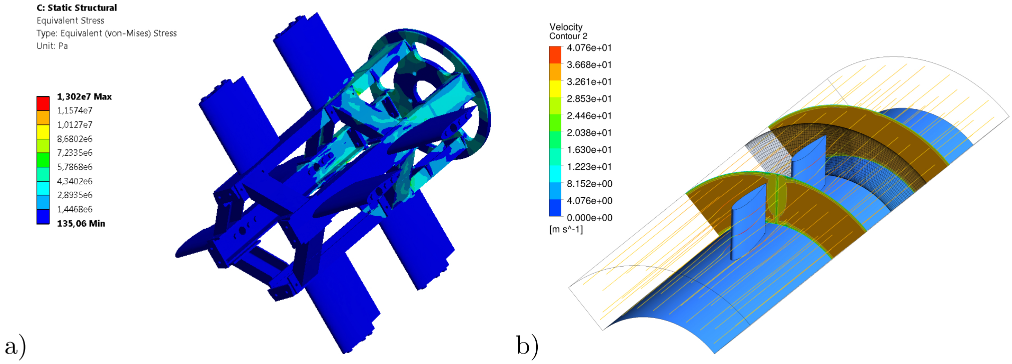

Figure 2.3.13: *a) Stress distribution from FEA of the internal structure together with the struts. b) CFD analysis of the turbine section without stator and rotor.*

Downstream of the struts, an annular screen is located to dissipate the wakes generated by the NACA 0015 struts. The screen has been dimensioned based on results from CFD analysis. In this simulation, a 90° sector of the turbine section (without stator and rotor) is modeled. Figure 2.3.13 shows the how the wake after the first strut is dissipated in the screen. Therefore, a screen with the same pressure drop ($K = 1.41$) as the one used in the simulation was selected (cell width of 2 mm, wire diameter of 1 mm).

2.3.5.2 Braking system

A hydraulic brake system controls the turbine rotational speed. A hydraulic pump connected to the rotor disk through its shaft generates the torque required to control the speed. The oil is then pressurized from 1 to a maximum of 350 bar. This pressurized oil passes through needle valves that restrict and regulate the flow. The mechanical power losses in the pressure system are transformed to heat power which is dissipated through an oil-water heat exchanger connected to a water based cooling system. This brake system is meant to work up to on-design rotational speed and torque conditions (see Table 2.3.3) and off-design cases where higher load is transferred to the rotor shaft.

There are other possibilities for controlling the rotational speed of the turbine and transferring load to the shaft. Electric generators are most common for this purpose in these kind of facilities, but there are several advantages of having a hydraulic system. First of all, a hydraulic pump is more compact. Since the hub inner radius is about 320 mm long, the size of the equipment is an important constraint. In addition, a hydraulic pump is simpler to install than an electric generator because there is no need for dimensioning bearings or having a stiffer structure that can stand the heavy weight of the electric equipment (77 kg [18] vs more than 1000 kg [19]). Furthermore, the price of this electric equipment is higher than the hydraulic system. On the other hand, regulating speed and torque is more accurate using an electric generator, and there is the possibility of transferring the energy from the turbine to the centrifugal fan, therefore giving a more energy efficient facility.

2.3.5.3 Turbine stage

The turbine stage is the source of realistic boundary conditions to the EES test section where aero and heat transfer measurements will be performed in the future. The main parameters of this turbine stage are summarized in Table 2.3.3. The Reynolds number at on-design conditions is representative of a compromise case between large turbofan engines and geared engines.

Parameter	**Value**
Re number based on channel height	465,000
Shroud radius [m]	0.553
Hub radius [m]	0.34
Axial velocity [m/s]	32.8
Mass flow rate [kg/s]	22.8
Temperature [K]	300
Flow coefficient (Ca/U)	0.76
Load coefficient ($\Delta H/U^2$)	1.62
Rotor exit flow angle	-35°
Pressure ratio	1.037
Number of NGVs	60
Number of rotor blades	72
Rotational speed [rpm]	920
Torque [N.m]	710
Power [kW]	68.4

Table 2.3.3: **Turbine stage parameters for on design conditions.**

In a real engine, the flow into the EES is characterized by the swirl velocity coming from the rotor, wakes generated by the stator and rotor, tip leakage flow and purge flow coming from the hub. Hence, not only LPT dimensionless parameters should be representative of real engines but also the geometric features such as P-flange pocket, tip seal and purge flow through rim seals. Figure 2.3.14 shows a detailed view where these features can be seen.

2.3.5.4 Aero design of the turbine stage

The LPT aero design was done at GKN Aerospace Sweden. Stator and rotor blades were designed using 3D methods, rendering complex geometries. Figure 2.3.15 shows a 3D image of these components. There are 60 NGVs and 72 rotor blades in the turbine stage and 12 OGVs in the EES. The purpose of having this combination is to perform CFD analysis of the full turbine stage together with the EES using periodic boundary conditions over a 30° sector (five NGVs , six rotor blades and one OGV). The computational time required for any CFD analysis is therefore significantly decreased.

Furthermore, a tip seal was designed to obtain a realistic mass flow leakage over the rotor stage. Tip leakage flows influence flow on the EES creating rolling vortices on

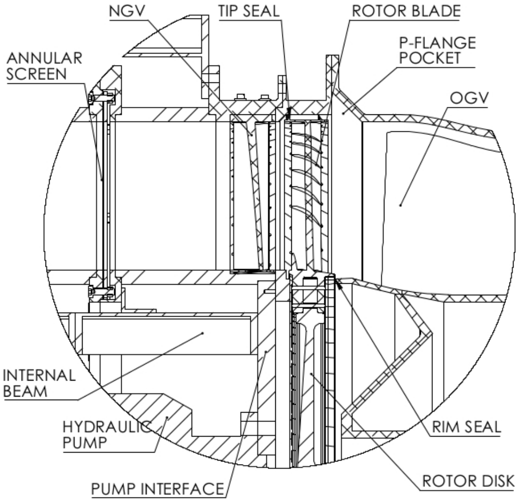

Figure 2.3.14: *Detailed view of the turbine stage cross section.*

the surface of the vanes located at the outlet of a turbine (see Rojo et al. [20]) and considerably increase the heat transfer rate.

For the design of the tip seal, the main requirement is to obtain a mass flow leakage between 0.5% and 1% of the total mass flow coming to the turbine stage. Furthermore, since the turbine must be engine like, the tip seal design should be similar to the existing one in aero engines. CFD tools were used to design this seal. A 2D axisymmetric design process was followed under the next assumptions:

- The flow exits the stator with the same swirl angle as the NGV's outlet angle.
- The rotor does not affect the flow at the inlet to the tip sealing. Therefore, fixing a given pressure drop representative of on design operating conditions is sufficient

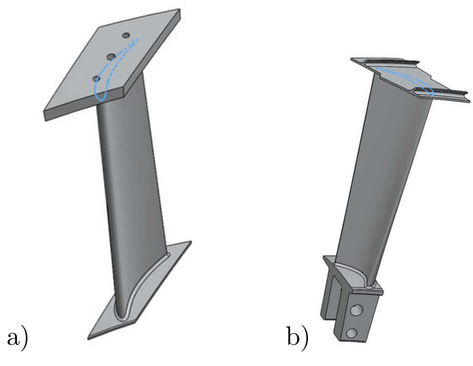

Figure 2.3.15: *a) NGV. b) Rotor blade.*

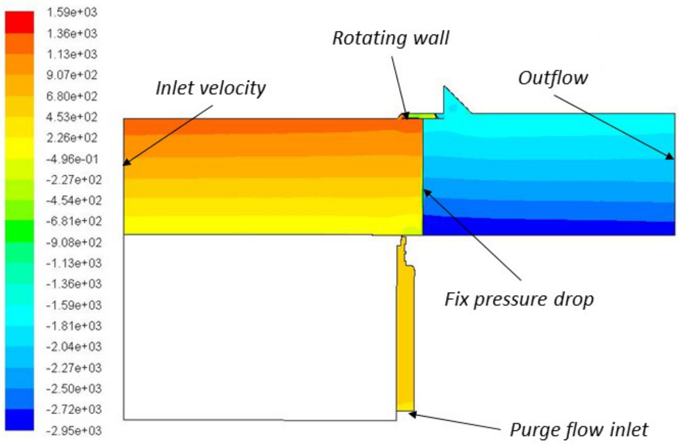

Figure 2.3.16: *Pressure drop distribution for the 1.5 mm tip to shroud minimum distance case.*

enough to provide realistic boundary conditions.

Figure 2.3.16 shows the pressure distribution together with the boundary conditions applied. For the geometry parametrization, ANSYS Workbench was used as a meshing tool and the 2D axisymmetric simulations (including swirl flow) were performed in FLUENT. The turbulence model used was $k - \omega\ SST$ and the low Reynolds wall treatment since $y^+ < 1$.

The first conclusion drawn from this analysis was that adding more ribs does not necessarily improve the sealing performance. Figure 2.3.19 shows the comparison between two designs with two and three ribs, respectively. Different flow patterns were found for the two rib seal case, changing the tip seal to shroud distance as shown in Fig. 2.3.17. There is no such change in the flow in the three rib seal(see Fig. 2.3.18). The last conclusion was that the flow from the rotor does not create a major recirculation at the outlet of the tip seal.

2.3.5.5 Mechanical design of the turbine stage

Designing a rotating turbine requires an analysis of the loads transported from the fluid to the solid rotor. It is important to understand the main hazards for the rotor's integrity and operational stability. The most representative failure modes are listed below.

- Static loads. The action of aero loads on the rotor blade, fasteners and disk could lead to blades exiting the turbine section or disk burst. For this reason, static analysis was performed.
- Thermal load. Creep and changes in geometry due to thermal loads can lead to contacts between the rotor and the surroundings, high local stresses or degradation

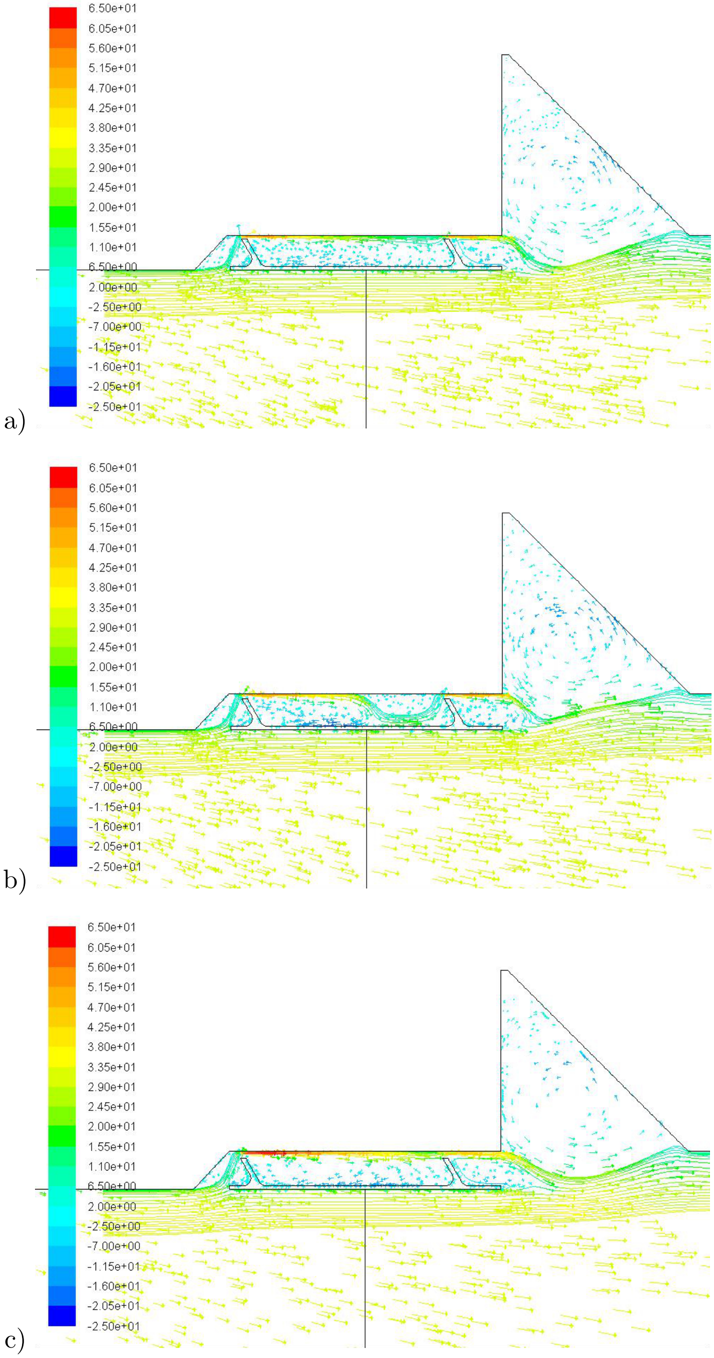

Figure 2.3.17: *Tip seal design with two ribs. Path lines and vector velocity plot colored by axial velocity for tip to shroud distances of a) 1 mm, b) 1.5 mm and c) 2 mm.*

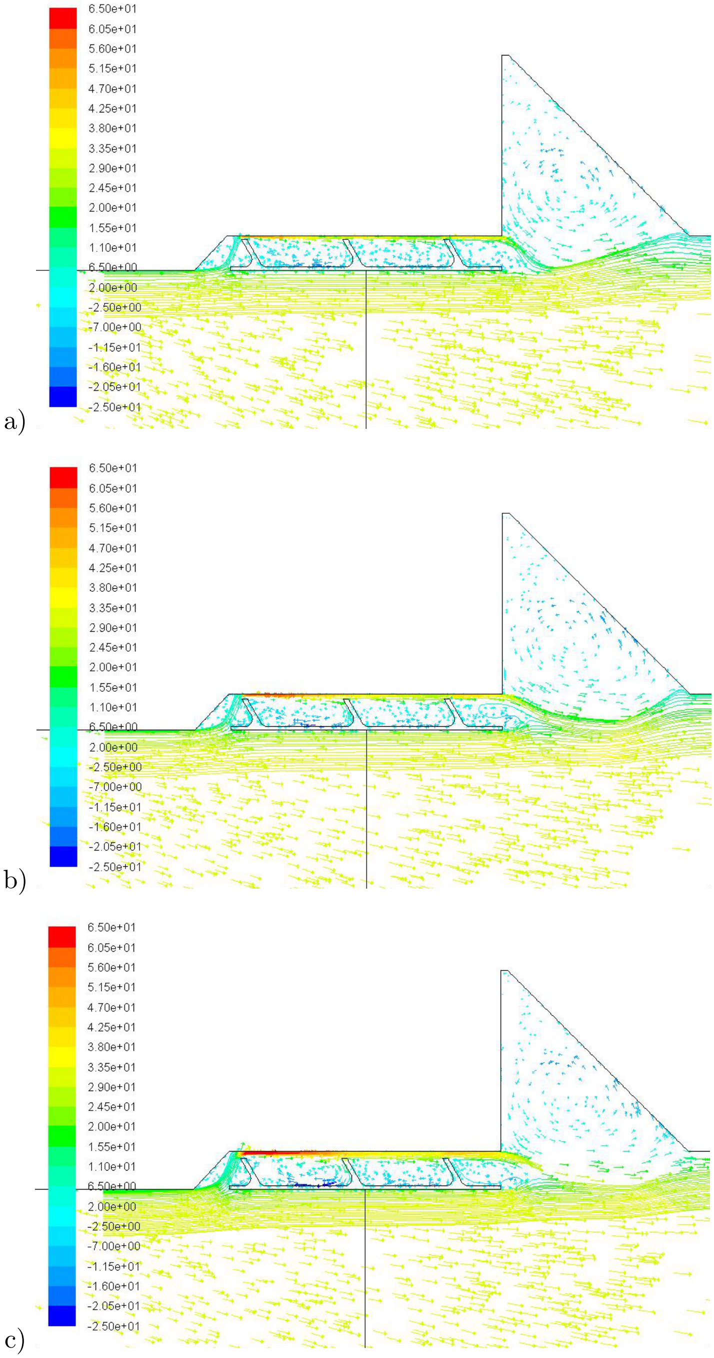

Figure 2.3.18: *Tip seal design with three ribs. Path lines and vector velocity plot colored by axial velocity for tip to shroud distances of a) 1 mm, b) 1.5 mm and c) 2 mm.*

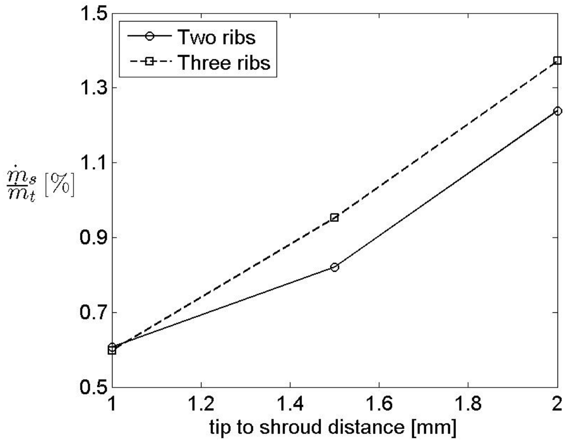

Figure 2.3.19: *Comparison of two designs based on the mass flow ratio between the mass flow that goes through the sealing and the total mass flow at the inlet.*

of the material's mechanical properties. The turbine operates at room temperature or slightly higher. The maximum temperature will be at the rotor shaft, where it is expected to be about 60°C. Hence, there is no need to include this load in the mechanical study.

- Vibrations. Most of the loads applied to the rotor have an unsteady component. This unsteady load could lead to excitation of the rotor or the structure and, in the worst case, a break-down of the turbine section.

- Fatigue. Mechanical properties of some materials change dramatically when the loads applied are cyclic. For example, since the turbine rotates at almost 1000 rpm, during one run of five hours, $3 \cdot 10^5$ load cycles are applied to the rotor. HCF and LCF studies have been done to find a way to avoid this failure mode.

Regarding the source of loads, the most important loads are the aero loads, which act mainly in the tangential and axial directions, and the centrifugal load which is mainly applied in the radial direction. Even though the loads could be simplified into a combination of these loads, the geometry is highly three-dimensional. Therefore, FEA must be performed in order to obtain realistic stresses and deformations over the turbine blade. Figure 2.3.20 shows a 5° rotor sector FEA at on-design conditions.

Furthermore, a modal analysis was made in order to obtain the first ten resonance frequencies of the rotor. Afterwards, with knowledge of these frequencies and the main excitation sources, a Campbell diagram was constructed to assess potential resonance vibration problems. Figure 2.3.21 shows the diagram.

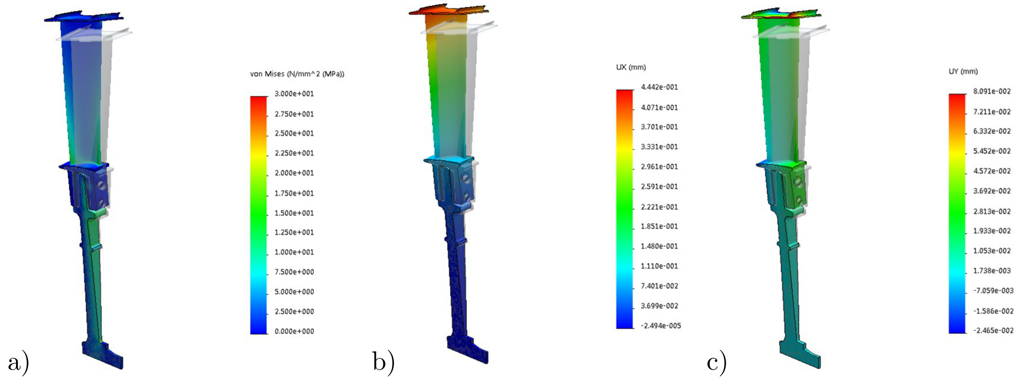

Figure 2.3.20: *Results of static stress FEA analysis of 5° rotor sector at on-design conditions. a) Stress distribution, b) axial displacement and c) radial displacement. Deformation scale factor of the deformed geometry is 120.*

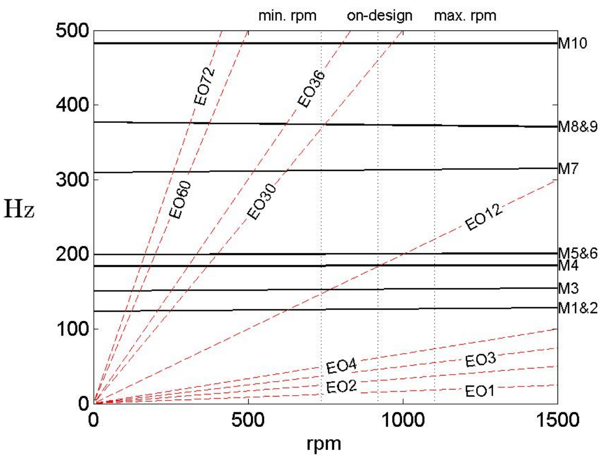

Figure 2.3.21: *Campbell diagram of the rotor turbine.*

2.3.6 Engine exit structure

The aero design of the EES was done at GKN Aerospace Sweden using an in-house code. Figure 2.3.22 shows a 3D view of this component.

There are 12 OGVs in the EES and a pipe for purge flow injection is included in the design. There will be a realistic P-flange pocket located at the beginning of the shroud, upstream of the leading edge of the OGVs.

These experiments will be performed by means of a five-hole probe, a seven-hole probe and an IR camera. The use of the IR thermography for flow visualization purposes will be investigated.

This component has practical use in this facility since it is designed to remove the

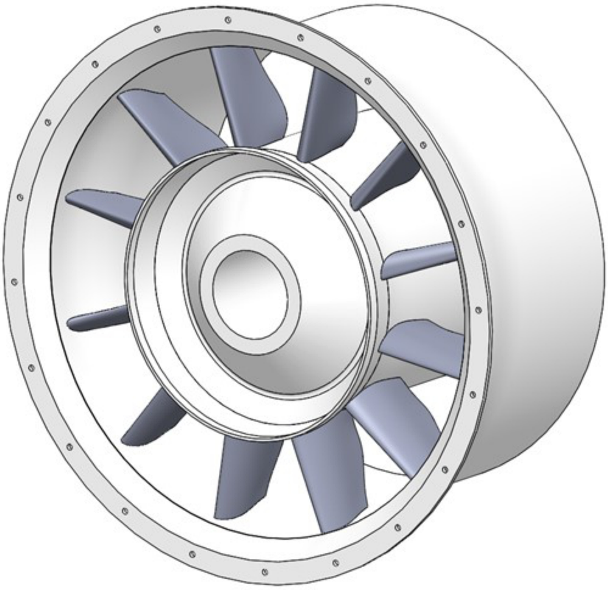

Figure 2.3.22: *Aerodesign of the EES.*

swirl coming from the LPT, and therefore, obtain an axial flow at the outlet. As part of the study of the total dynamic pressure of the flow at the outlet in this project, several OGV designs will be tested since, in a real aero engine, some of the OGVs have different features, such as bumps at the hub and shroud.

2.4 Pressure drop calculation

The design of these kinds of facilities requires a continuous design loop where one of the most important parameters to take into consideration is the total pressure drop in the facility. For this facility (and most of low-speed wind tunnels), there is a trade-off between reaching the highest Reynolds number possible in the test section and the size of the facility and power of the motor unit that drives the flow. In this case, the limitations are a 200 kW of electric and cooling power supply and the space available in the lab (7 m height, 4 m width and 14 m length). Once the turbine parameters are set, the Reynolds number in the test section and the mass flow rate are known. When previous limitations are taken into consideration, one can start calculating the pressure distribution for different rig concepts.

Empirical correlations and/or CFD tools were used for each component to calculate the pressure drop. These empirical correlations are summarized in Barlow et al. [9]. In addition, pressure measurements where performed in the flow conditioning of a similar annular-cascade rotating rig at Chalmers University of Technology (see Arroyo et al. [12]). In these data, correlations were obtained for the pressure drop coefficient of turbulence

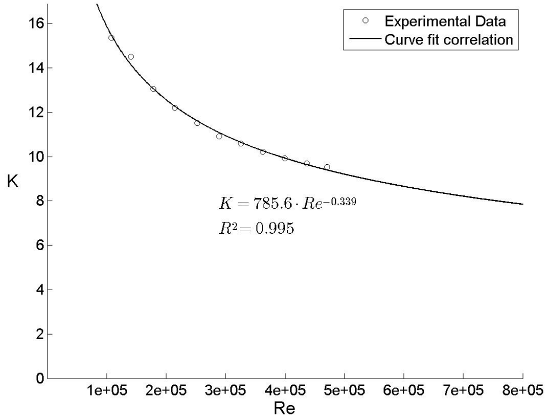

Figure 2.4.1: *Measured pressure drop coefficient for a turbulence screen. Wire diameter and cell width of 0.33 and 1.25 mm respectively.*

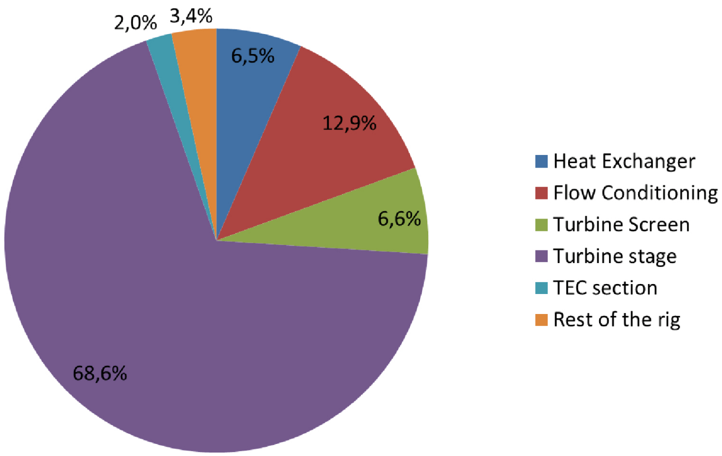

Figure 2.4.2: *Pressure losses chart.*

screens, as shown in Fig. 2.4.1. These correlations showed a larger pressure drop coefficient compared to what would be expected from older correlations. An explanation for this anomaly could be that dust had accumulated in the screens (especially over finer screens) and honeycomb.

There are two main outcomes off this analysis with regard to the sizing of the rig and the location of different components. First, the heat exchanger should be located where there is the largest cross section area because the losses are proportional to the square velocity and the pressure drop coefficient is the highest in the entire facility. The second outcome is that the size of the flow conditioning ducts should be at least 2 m in diameter to produce less than 10% losses in this section. Figure 2.4.2 shows the main sources of pressure loss inside the rig. This and the intention of diffusing the flow without placing turbulence screens, show is the need to have such a long diffusing section.

3 Conclusions

This thesis presents three years of work at Chalmers University of Technology on the design of a large-scale low-speed LPT rig. The rig was designed using experimental data from classical low-speed wind-tunnel literature, experimental data from measurements made in an existing rig and numerical tools; these are cases in which none of the experimental correlations can provide an exact solution.

A new method for axisymmetric design of a contraction duct and a central body was developed. In addition, by means of CFD tools, the pressure loss coefficient of the contraction section was calculated for all operating points of the facility and add precision to the measurement of mass flow.

FEA analysis was done in the most loaded components and modal analysis in the rotor turbine. Through these analyses, the safety of the rig was checked. Moreover, the deformations of the structures were checked in order to guarantee that the deformations will not interact with the flow quality negatively, i.e. producing asymmetries in the flow velocity distributions.

Although heat transfer measurement techniques have not been mentioned in this report, an IR thermography technique was developed during these years at Chalmers University of Technology using an in-house code.

Finally, the rig is expected to be operative by April 2016 and, with the data acquired in this rig, a better understanding of the flow inside this section will lead to lighter structures and more environmental friendly engines.

3.1 Future work

The project will continue with the manufacturing and assembly of the turbine section and connection of the brake and cooling systems. In addition, mechanical design of the EES and traversing system will be carried out. The rig will start to be commissioned.

Future experimental work will also focus on measuring and characterizing the flow inside the EES. Some examples of measurement techniques that will be used are listed below:

- Measurement of total pressure, velocities, velocity angles and turbulence at the inlet of the LPT and EES.
- Measurements of total and static pressure, velocities and velocity angles and turbulence at the outlet of the EES, obtaining a 2D plane. Furthermore, wake profile measurements (total pressure and velocity angles), detailed profiles at a few sections.
- Detailed study of end-wall boundary layers. Boundary layer sizes must be measured.
- Static pressure measurements on OGVs, end-walls and bumps.
- Transition measurements of interest.
- Oil flow visualization technique over the OGVs, hub and shroud.

- Heat transfer measurements inside the EES section.

4 My Contributions

4.1 Paper 1

In paper 1 I participated in the aero and mechanical design of the LPT-OGV rig located at Chalmers University of Technology. For this work, I had the collaboration of research assistants that focused on the mechanical design of the rig. The actions taken by me are listed below:

- Aero design of the LPT-OGV rig.
  - Design of the diffusing section by means of experimental correlations and CFD tools.
  - Design of the flow conditioning section and selection of components.
  - Development of a new 1D method to obtain the geometry contraction duct for a given central body in it.
  - CFD analysis of the annular section upstream of the turbine.
  - Design of the rotor blade tip sealing.
- Mechanical design of the LPT-OGV rig.
  - Layout of the rig.
  - FEA on the rotor, turbine structure and contraction section.

The manufacture of the hardware was done by external workshops. The aero design of the NGV and rotor blade was done at GKN Aerospace Sweden.

4.2 Additional work

This licentiate is focused on the design of a low-speed large-scale annular-cascade rig with a rotating turbine upstream the test section. At the same time, I developed in parallel heat transfer measurement techniques which lead to the publication of 4 papers.

The first paper (Rojo et al. [20]) shows the experimental work performed in a low-speed large-scale annular-cascade turbine rig at Chalmers University of Technology. The purpose of this experiment was to measure the heat transfer coefficient on a loaded guide vane located inside an ITD downstream of a HPT by means of IR thermography. Experimental data was compare with CFD data from steady RANS simulations.

The second paper (Rojo et al. [5]) shows the design of an instrumented endwall for heat transfer measurements in a low-speed large-scale linear cascade facility located at Chalmers University of Technology. This paper shows the influence of the Reynolds number and inlet flow angle on the heat transfer on the linear cascade endwall.

In addition, I participated in an IR measurement campaign in pulsating impingement jets on an inclined surface. The results of this collaboration led to two publications with me as the second author (see Bovo et al. [21] and Bovo and Rojo [22]).

During this time, I have supervised four Master theses, on of which led to the publication of one paper. The others were focus on development of tools and methods that will be use in the LPT-OGV rig (see Jimenez (2013) [23], Llacer (2014) [24], Barrachina (2014) [25] and Urbiola (2015) [26]).

Bibliography

[1] http://www.aircraftenginedesign.com/pictures/gp7000.gif. Accessed 1-October-2015.

[2] R. Goldstein and R. Spores, “Turbulent transport on the endwall in the region between adjacent turbine blades,” *Journal of Heat Transfer*, vol. 110, no. 4a, pp. 862–869, 1988.

[3] J. Hjärne, J. Larsson, and L. Löfdahl, “Design of a modern test-facility for lpt/ogv flows,” in *ASME Turbo Expo 2003, collocated with the 2003 International Joint Power Generation Conference*, pp. 137–145, American Society of Mechanical Engineers, 2003.

[4] J. Hjärne, *Turbine outlet guide vane flows.* PhD thesis, Chalmers University of Technology, 2007.

[5] B. Rojo, C. Jimenez, and V. Chernoray, “Experimental heat transfer study of endwall in a linear cascade with ir thermography,” in *EPJ Web of Conferences*, vol. 67, p. 02100, EDP Sciences, 2014.

[6] F. Schönleitner, H. Koch, T. Selic, M. Hoeger, and A. Marn, “Comparison of the experimental results between a 2d egv cascade test and a rig test under engine representative conditions,” in *ASME Turbo Expo 2014: Turbine Technical Conference and Exposition*, pp. V02CT38A053–V02CT38A053, American Society of Mechanical Engineers, 2014.

[7] C. Arroyo, *Aerothermal investigation of an intermediate turbine duct.* PhD thesis, Chalmers University of Technology, 2009.

[8] P. Bradshaw and R. Pankhurst, “The design of low-speed wind tunnels,” *Progress in Aerospace Sciences*, vol. 5, pp. 1 – 69, 1964.

[9] J. Barlow, W. Rae, and A. Pope, *Low-Speed Wind Tunnel Testing.* Aerospace engineering, mechanical engineering, Wiley, 1999.

[10] R. D. Mehta and P. Bradshaw, “Design rules for small low-speed wind tunnels,” 1979.

[11] J. Groth and A. V. Johansson, “Turbulence reduction by screens,” *Journal of Fluid Mechanics*, vol. 197, pp. 139–155, 1988.

[12] C. Arroyo, L.-U. Axelsson, U. Håll, T. G. Johansson, J. Larsson, and F. Haselbach, “Large scale low speed facility for investigating intermediate turbine duct flows,” in *44th AIAA Aerospace Sciences Meeting and Exhibit, AIAA-2006-1312*, 2006.

[13] T. Morel, “Comprehensive design of axisymmetric wind tunnel contractions,” *Journal of Fluids Engineering*, vol. 97, no. 2, pp. 225–233, 1975.

[14] M. Mikhail, “Optimum design of wind tunnel contractions,” *AIAA journal*, vol. 17, no. 5, pp. 471–477, 1979.

[15] M. Abbaspour and M. Shojaee, "Innovative approach to design a new national low speed wind tunnel," *International Journal of Environmental Science & Technology*, vol. 6, no. 1, pp. 23–34, 2009.

[16] R. D. Mehta and J. H. Bell, "Boundary-layer predictions for small low-speed contractions," *AIAA journal*, vol. 27, no. 3, pp. 372–374, 1989.

[17] G. Chmielewski, "Boundary-layer considerations in the design of aerodynamic contractions," *Journal of Aircraft*, vol. 11, no. 8, pp. 435–438, 1974.

[18] http://www.parker.com/. Accessed 13-October-2015.

[19] http://www.brookcrompton.com/. Accessed 13-October-2015.

[20] B. Rojo, V. Chernoray, M. Johansson, and M. Golubev, "Experimental heat transfer study in an intermediate turbine duct," in *49th AIAA/ASME/SAE/ASEE Joint Propulsion Conference*, 2013.

[21] M. Bovo, B. Rojo, and M. Golubev, "Measurements of a single pulse impinging jet. a cfd reference," in *EPJ Web of Conferences*, vol. 67, p. 02010, EDP Sciences, 2014.

[22] M. Bovo and B. Rojo, "Single pulse jet impingement on inclined surface, heat transfer and flow field," tech. rep., SAE Technical Paper, 2013.

[23] C. Jimenez, "Experimental heat transfer studies with infrared camera," 2013.

[24] S. Llacer, "Design of instrumented end-wall for heat transfer measurements in a low-speed linear cascade and ow measurements," 2014.

[25] A. Barrachina, "Heat transfer studies with ir thermography techniques," 2014.

[26] C. Urbiola, "Experimental heat transfer measurement technique validation and measurements in a linear cascade of an ogv and endwall," 2015.

Paper 1

FACILITY FOR INVESTIGATING THE FLOW IN A LOW PRESSURE TURBINE EXIT STRUCTURE

B. Rojo - D. Kristmundsson - V. Chernoray

Applied Mechanics, Chalmers University of Technology, Göteborg, Sweden
borja.rojo@chalmers.se, darri.kristmundsson@chalmers.se, valery.chernoray@chalmers.se

C. Arroyo - J. Larsson

GKN Aerospace Engine Systems Sweden, Trollhättan, Sweden
carlos.arroyo@gknaerospace.com, jonas.larsson@gknaerospace.com

ABSTRACT

This paper presents the design of a turbine facility for the investigation of the flow in the engine exit structure (EES) at Chalmers University. The EES is the structure located downstream of the low-pressure turbine in a jet engine. In the current facility, in order to generate realistic inlet boundary conditions for the EES, an LPT stage is located upstream of the EES. The facility is a large-scale, low-speed annular cascade, and the flow Reynolds number based on the channel height in the turbine stage is 465,000, which is representative for large turbofan engines.

The design of the facility follows classical low speed wind tunnel design. Experimental correlations obtained from data collected in a previous rig and from previous studies in low-speed wind tunnels have been used to compute pressure losses. CFD has been used in the design of the facility.

NOMENCLATURE

A amplitude of the acceleration function
EES engine exit structure
FEA finite element analysis
K pressure drop coefficient
L contraction length
LPT low pressure turbine
NGV nozzle guide vane
OGV outlet guide vane
Re Reynolds number
S cross-section area
a acceleration of the flow
c distance from contraction inlet to beginning of damping function
d distance from contraction inlet to end of damping function
$\dot{m}$ mass flow
p distance from contraction inlet to nose cone
u mean velocity in axial direction
y^+ dimensionless wall distance
β screen porosity
κ parameter for acceleration function
λ parameter for acceleration function
ρ density of air
ω turbulence frequency
R_{cb} radius of the central body

INTRODUCTION

Demands from industry to improve the efficiency of energy systems, including aero engines, are leading to a research focus on more efficient propulsion systems. Energy efficiency can be increased in jet engines by increasing the by-pass ratio or introducing geared engines. As a consequence, LPT OGV inlet swirl angles are increased for ungeared two-spool engines or geared engines have increased off-design swirl variations. Therefore, LPT OGV aerodesign is becoming more demanding and new experimental data on these novel OGV designs are required.

OGVs are located downstream of the last stage of the LPT in an aero engine. The main purpose of this component is to connect the external casing and the core. The OGVs thus carry the loads from the internal to the external structure. Furthermore, OGVs provide access for oil tubes, oil-scavenge and electrical cables from the outer case to the shaft of the engine. In addition to the structural and connective functions, the OGVs also play an important aerodynamic role in an aeroengine because they eliminate the swirl that comes from the LPT situated upstream.

The flow around an OGV is inherently complex, involving wakes from the upstream turbine (see Goldsteain and Spores, 1988), interaction of boundary layers and the risk of flow separation. Due to the small number of OGVs in the EES (typically 12) secondary flows become very important to study. Furthermore, structural requirements on the EES lead to the use of polygonal endwalls and sunken engine mounts and, therefore, complicating the aero design in the shroud region. The design parameters that are required from an aerodynamic point of view are minimization of the pressure drop and the capability to withstand flow separation. Moreover, the prediction of flow separation and heat transfer becomes more crucial when the OGV has an inlet incidence angle different from the on-design operation condition. Modern geared engines show large swirl angle variations and high temperatures at off design conditions, hence, heat transfer predictions become critical and relevant validations from this type of rig are needed.

Although experimental data of the flow in the EES and outlet guide vanes exists, these data are insufficient for CFD validation. Most of the experimental data available for flow around OGVs are either representative of old OGV designs or collected from experiments in linear cascades (see Hjärne et. al., 2003, Hjärne, 2007 and Rojo et al., 2014), which are valuable for 2D validations. Recently, Schönleitner et al. (2014) showed that an annular cascade rig with an LPT upstream of the test section can provide realistic data on the complex flow inside the EES. In addition, it is of great interest to study large variations from on-design conditions at the inlet of the OGVs, as OGVs should be able to withstand these variations inside a aero engine.

Finally, it is important to point out that, even though current LPTs operate close to sonic conditions, most of the physical phenomena involved in the EES section are present also at low speed such as secondary flows, rotating wakes and interaction with the duct endwalls. Hence, the experimental data obtained from this annular cascade rig can be valuable for CFD validation and component testing. Furthermore, building a high-speed rig would have become expensive, difficult to operate and very high requirements on the measurement techniques would have been imposed.

RIG LAYOUT

Description

Figure 1 shows the rig layout. The air flow is run by a centrifugal blower. There is a long duct (length to width ratio of 2.7) at the outlet of the fan in order to settle the flow from the centrifugal fan and obtain better flow uniformity with minimal losses at the first corner and the long diffuser duct (first diffuser duct). The diffusing angle for the first and second diffuser ducts have been selected to be as low as possible in order to reduce the risk of large separations and unsteady flow in the diffuser. The second and third corners are located downstream of the first and second diffuser ducts, respectively.

A heat exchanger is located downstream of the third corner. The heat exchanger is required to

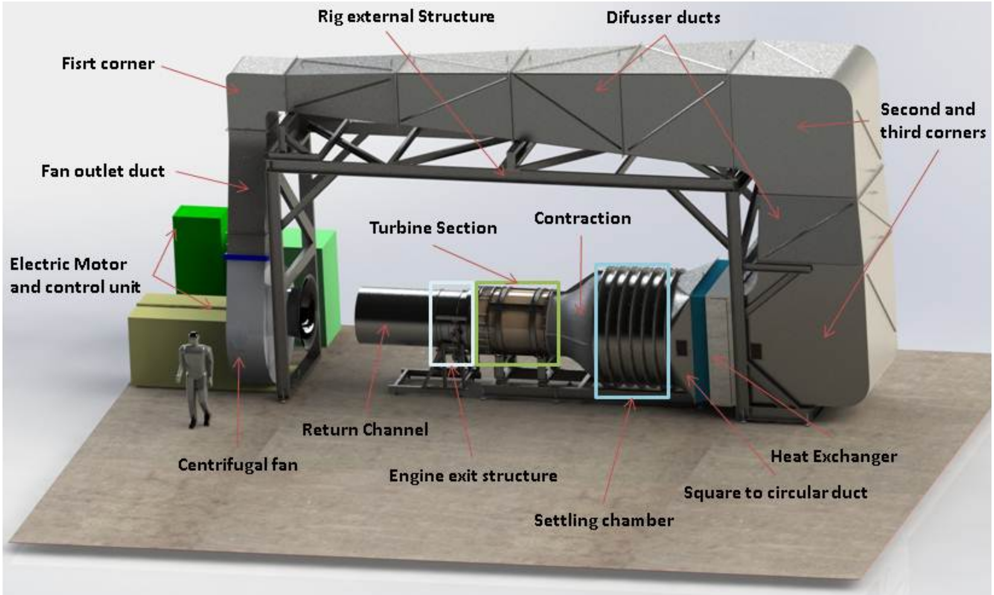

Figure 1: **Experimental facility**

control the temperature in the rig so that it is possible to achieve steady state at approximately 30°C. In addition, this component creates the largest pressure loss of all components (not taking into account the turbine) which requires a location in the section where the cross section area is largest in the rig. One way to recuperate or make good use of the losses produced by the heat exchanger is by locating it upstream of the settling chamber due to the fact that the pressure losses induce flow uniformity at the outlet of this component, creating less losses afterwards in the settling chamber and producing a more uniform flow.

In the settling chamber, a honeycomb and five screens are used to improve flow uniformity. The main purpose of having a honeycomb is to remove swirl flow by damping the cross flow velocity fluctuations. The screens make the flow uniform. Downstream of the screens, the contraction is formed by the outer casing and the central body. At the same time, the contraction allows for a section change from circular to annular, which is needed to connect the flow conditioning section to the LPT section.

Requirements for the facility

The main requirements of this facility are listed below.

- **Reynolds number similarity.** It is important to have a Reynolds number at the inlet of the turbine stage and EES section that is similar to what can be found in a real aero engine in order to achieve flow characteristics comparable with a real engine. In this facility, the Reynolds number is about 350,000 based on the axial chord of the OGVs. For large ungeared engines, the Reynolds number can be around 450,000 and, for a smaller engine like a geared turbofan engine, the Reynolds number can be over 300,000.
- **Stable operating conditions and repeatability.** In this experimental rig, it is required to have

a steady flow (velocity, pressure and temperature) into the turbine stage and EES. Furthermore, under same operating conditions same results should be obtained in this facility.

- **Representative inlet flow to the EES.** It is required that the flow from the turbine has prescribed wakes and secondary flows, swirl- and massflow-distributions, tip leakage flow and rim-seal purge flow. It should be possible to cover important off-design variations (from -25° to -45°) and vary swirl angles, massflow and Re numbers.

- **Access for the measurement techniques.** Access and traversing systems for the different measurement techniques should be provided while the disturbances to the flow should be kept to a minimum.

- **Modular design.** A modular design will enable the possibility of exchanging the EES and testing different configurations.

- **CFD Friendly.** To decrease the computational resources needed for CFD simulations, the ratio between the number of NGVs and/or rotor blades and OGVs should be a low integer number (in our case 60/72/12).

COMPONENTS

This section explains the function and design criteria of all the components described in the previous section in detail.[1]

Fan unit

A centrifugal fan was selected for providing the required flow rate and pressure. A frequency converter drives the motor and allows for a continuous regulation of the mass flow rate in the facility. Elastic connections are used between the fan and the rest of the facility in order to avoid propagating the vibrations of the fan to the neighbouring components. Table 1 shows the main characteristics of the fan unit.

Parameter	**Value**
Design volume flow rate [m^3/h]	6900
Design total pressure [kPa]	7.56
Fan wheel diameter [mm]	1620
Maximum rotational speed [rpm]	1800
Electric motor maximum power [kW]	200
Total efficiency	0.82
Noise levels [dB]	114.1

Table 1: **Fan main characteristics.**

Diffusing Section

The main purpose of having a diffusing section is to increase the cross section area from the fan outlet (a rectangular section of 710x900 mm) to a square section of 2000x2000 mm so that the pressure losses at the heat exchanger and the settling chamber become small enough to run the turbine with the selected centrifugal fan. The most important requirement for this section is to provide the area

[1] All the CFD simulations have been carried out using FLUENT, and ICEM ANSYS was used as a meshing tool.

change and turn the flow with minimum losses, flow separation and non-uniformities. An incorrect diffuser design can lead to high losses (due to flow separation and jet flow) and non-uniform flow which can propagate even through a settling chamber. In the current case this is prevented by adding turning vanes in the corners and by a diffuser design with a small diffuser angle (7.5°), which is the lowest angle that can be achieved with the space available. According to Barlow et. al. (1999), this angle is well below the flow separation margin, which is also supported by our CFD results.

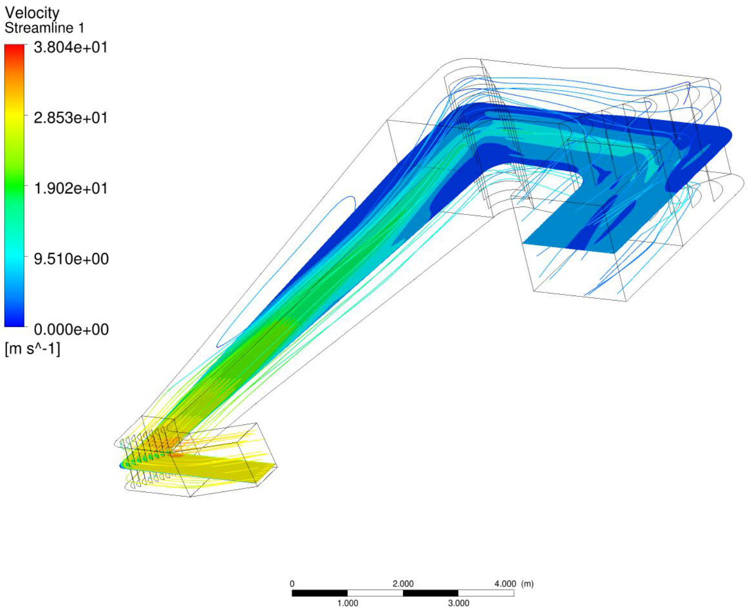

Figure 2: **Contour velocity plots of the diffusing section midplane and pathlines.**

Figure 2 shows a velocity contour plot of the midplane of this section. These are the results of a steady simulation with 6.7M cells and a y^+ value between 40 and 100 using the $k-\omega$ SST turbulence model. Uniform mass flow inlet boundary condition has been used. The convergence criteria has been set as maximum residual for continuity of 10^{-2} and for the rest of the variables 10^{-4} and residual flat lining. Typically, flow at the fan outlet is not uniform and this translates into a higher risk of flow separation in the actual facility. If the flow separation will be present in the actual rig, a screen will be placed in the first diffuser duct to prevent the separation.

In addition, the pressure drop produced by the heat exchanger is taken into account because it can affect the flow through the third corner. The heat exchanger has been simulated using a plane with a fixed pressure drop coefficient (radiator boundary condition in FLUENT). The pressure drop coefficient is calculated based on the manufacturer's pressure loss data.

Several cases of diffusing sections have been studied where a screen has been placed at different sections of the long diffuser duct to check how much it would improve the flow uniformity or even avoid possible flow separation in this section and to identify whether there is an optimum location for the screen. It was obtained that locating a screen in the middle of the diffuser with a pressure drop coefficient of 1.4 is optimal to make the flow uniform in this section, and could be used in the actual rig if flow separation would occur.

All the corners have been designed according to guidelines found in Barlow et al. (1999). These corners are equipped with guide vanes, which are bent plates with a 90° circular arc and a straight trailing edge. Due to the high Reynolds number at the inlet of these components (over 500000), the gap-chord ratio chosen for the guide vane design is 1:4. Therefore, the first corner contains eight vanes and the second and third contain six vanes. Figures 2 and 3 show the resulting velocity contour plots obtained with these designs.

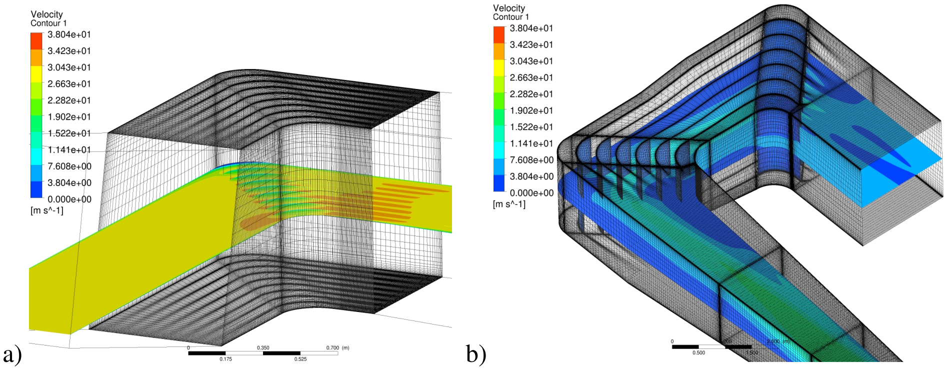

Figure 3: **a) First corner b) Second corner and third corner.**

Settling chamber

For several reasons, the flow coming out from the outlet of the last corner has a non-uniform velocity distribution. First of all, it is known that the flow coming out of a centrifugal fan is not perfectly uniform, but contains wakes and secondary flows. These flow non-uniformities might not be dissipated through the diffusing section. Furthermore, turning the flow creates non-uniformities such as wakes generated by the vanes or simply not turning the flow 90°(for example, overturning the flow due to a incorrect assembly of the vanes or geometrical tolerances). Looking at Figs.2 and 3, the effect of these components on the flow non-uniformities can be seen. Finally, the generation of a very low flow velocity on the sides and a high velocity jet in the middle can be seen in the diffuser ducts due to the adverse pressure gradient in the diffuser. In some cases, flow separation can occur in these ducts and disturb more the flow.

Screen number	**1**	**2**	**3**	**4**	**5**
Cell width [mm]	4	2.5	1.75	1.25	1
Wire diam. [mm]	1	0.7	0.5	0.33	0.24
β [%]	64	61	60	63	65
Wire Re	387	271	194	128	93
K	0.75	1.01	1.13	1.1	1.01

Table 2: **Main screen parameters. Pressure loss coefficient (K) calculated according to Barlow et al. (1999)**

All these factors together suggest the need of a flow conditioning section that has the purpose of giving a uniform flow at the outlet. Starting at the heat exchanger, the flow downstream of this section is expected to be improved because of the pressure drop generated by this component. After, there is a square to round section change whose length has been minimized with the help of CFD simulations, obtaining a length of 0.5 meter without having flow separation or generating large corner wakes.

A honeycomb is located downstream of the square to round section change. Honeycombs are used in large and small wind tunnels as effective flow straighteners. For our facility, the honeycomb chosen has hexagonal cells with a length of 110 mm and a hydraulic diameter of 14 mm. The length-to-cell diameter is around 8, which is the recommended ratio in Barlow et al. (1999).

In addition to this component, screens are needed. The reason for having these components is to reduce the flow non-uniformities in the axial direction and turbulence downstream of the honeycomb. According to Barlow et al. (1999), the best way to obtain a uniform flow is to have several screens instead of one very fine one. Table 2 summarizes the main parameters of these screens.

Contraction

The contraction connects the outlet of the settling chamber with the straight annular section of the turbine. This is done by placing a central body in front of the hub pipe and a contraction duct with a length of 1 meter.

Design criteria

The only function of this section is to drive the flow from a large radius section to an annular section with a smaller cross-sectional area. The requirements that the contraction must fulfil are listed below.

- **Minimum contraction length.** It is critical to design a short contraction so that there is enough space to place the turbine section and EES in the facility. Therefore, the first parameter that is taken into account is the length of the contraction.

- **Flow quality.** Generally, contractions are not sources of high pressure drops and, furthermore, the flow quality (from a wind tunnel perspective) can be increased if the contraction is correctly designed. In addition, one of the requirements of the turbine stage is to have uniform flow at the inlet of the NGVs. Hence, once the contraction has been designed, CFD techniques are used to check that the flow quality at the outlet is good enough for our purposes.

Design Method

In a literature search of this kind of contraction, no reports or examples of contraction design with a central body or a central body design criteria for contractions were found (see Morel (1975), Mikhail (1979), Abbaspour and Shojae (2009), Bell and Mehta (1988), Chmielewski (1974)).

In current design method of the contraction geometry it is assumed that the flow is incompressible, inviscid, irrotational and axisymmetric. Furthermore, only the mean axial speed and acceleration of the fluid are analysed (1D problem).

$$a(x) = u\frac{\partial u}{\partial x} \tag{1}$$

Using all the assumptions listed above, the expression for the flow acceleration becomes as shown in Eq. 1.

This could lead to an analytic solution in simple cases, i.e. axisymmetric contraction design without a central body based on a continuous acceleration function (see Chmielewski, 1974). Unfortunately, the central body produces a discontinuity in the acceleration function.

Furthermore, the acceleration function that provides the best shape for the duct and central body is not known. The following acceleration function has been used which is similar to the function used

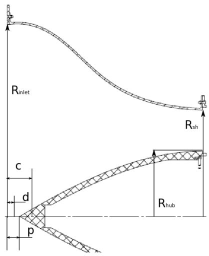

Figure 4: **Cross-section of the contraction.**

by Chmielewski (1974) for a contraction without central body.

$$a(x) = A \cdot f(x) = A \cdot \left[\sin\left(\frac{\pi x}{L}\right)^{\kappa}\right]^{\lambda} \tag{2}$$

Where $x \in [0, L]$ and $f(x) \geq 0$ for all x inside this interval. κ and λ are parameters and A is a constant. Now, the next step is to calculate the value of the constant A (or amplitude of the function). In order to calculate this value, it is necessary to integrate eq.1.

$$u(x) = \sqrt{2A \int_0^x f(x)dx + {u_0}^2} \tag{3}$$

Equation 3 is also used later for the calculation of the velocity distribution through the contraction. The velocity at the outlet is found using the mass conservation equation. A is calculated with eq.4.

$$A = \frac{u(L)^2 - {u_0}^2}{2\int_0^L f(x)dx} \tag{4}$$

Looking at eqs. 3 and 4 it can be seen that the only restriction on the definition of the function is that it must be integrable, which means that this method can be used even if $f(x)$ is not continuous. In the case of a central body, the acceleration function will be integrable but not continuous. To define the acceleration function, a set of three parameters is added: d, p and c (see fig. 4). It is first kept a constant acceleration below the ideal curve so that it damps the effect of the central body on the calculation of the contraction duct. Hence, from d, the acceleration is kept constant. Parameter p shows where the nose cone should be located. Finally, c represents where the value of the acceleration without a central body and the value of the acceleration with a central body are the same.

The acceleration function can thus be defined as follows:

$$f(x) = \begin{cases} \left[\sin\left(\frac{\pi x}{L}\right)^{\kappa}\right]^{\lambda} & \text{if } 0 \leq x \leq d \cup x \geq c \\ f(d) & \text{if } d < x \leq p \\ f(c) & \text{if } p < x < c \end{cases} \tag{5}$$

It is important to point out that, with this method, only the duct shape is calculated based on the acceleration curve. The central body is designed using a 3rd order polynomial. The boundary conditions for the polynomial are listed below.

$$B.C\ for\ R_{cb}(x) = \begin{cases} R_{cb}(x = p) = 0 \\ \left|\frac{dR_{cb}(x)}{dx}\right|_{x=p} = s \\ R_{cb}(x = L) = R_{hub} \\ \left|\frac{dR_{cb}(x)}{dx}\right|_{x=L} = 0 \end{cases} \tag{6}$$

In our case we select $s = 0.6$ and $p = 0.05$ to obtain a smooth shape that does not have an inflection point.

Finally, the geometry of the duct is calculated using the mass conservation equation for incompressible flow.

$$S = \frac{\dot{m}}{\rho u} \tag{7}$$

$$R(x) = \begin{cases} \sqrt{\dfrac{\dot{m}}{\pi \rho u}} & \text{if } x \le p \\ \sqrt{\dfrac{\dot{m}}{\pi \rho u} + R_{cb}(x)} & \text{if } x > p \end{cases} \tag{8}$$

A 2D axisymmetric CFD simulation was performed in order to validate the performance of the designed contraction shape. The CFD results are shown in Fig. 5. It was concluded that the contraction fulfils all our demands in terms of flow quality (no flow separation and less than 1% flow non-uniformity at the contraction outlet) and length (1 meter long).

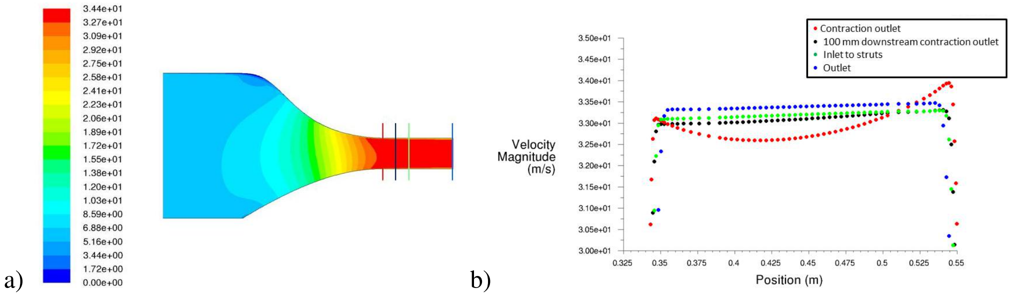

Figure 5: **a) Velocity contour plot of half a contraction section. b) Velocity profile at the exit of the contraction at different positions.**

TURBINE SECTION

As mentioned, the purpose of the turbine stage is to provide realistic inlet boundary conditions to the EES. Figure 6 shows a cross-sectional view of the turbine section.

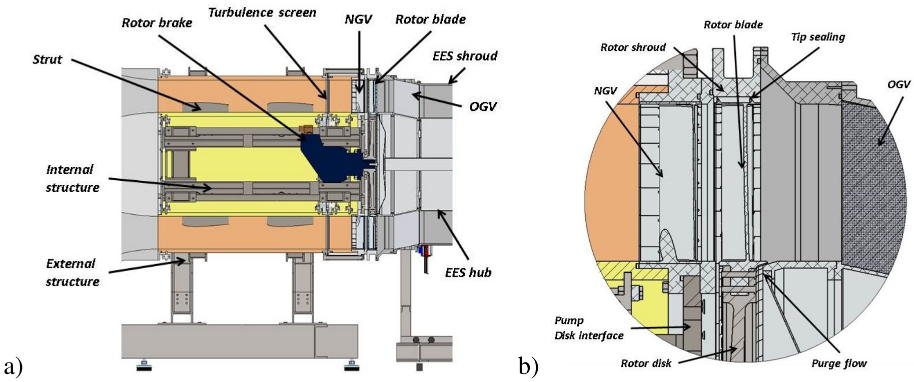

Figure 6: **a) Cross-sectional view of the turbine section. b) Detailed view of the turbine stage.**

Struts

There are two rows with four NACA 0015 profile struts, each made in steel. The axial chord distance of these airfoils is 300 mm and therefore they have a 45 mm maximum thickness. These struts have two different uses.

First of all, they are used for structural purposes. The turbine section is composed of external and internal structures that are concentric with each other. They must be connected through these struts, which are stiff enough to withstand all the load without suffering large deformations; at the same time, they do not disturb the flow, which must be uniform at the inlet of the turbine section. CFD analysis was used to check the size of the wakes generated by these struts. These wakes disturb the flow a total of 10° on the azimuthal direction. Furthermore, a screen (square cell width = 2mm, d = 1 mm, β=53% , K=1.41) is placed downstream of the last row of struts in order to dissipate the wakes and obtain uniform flow again. In addition, FEA was run to check whether the internal structure, the struts and the external structure can withstand the static loads. The result of FEA is that the minimum factor of safety on these structures is 24.

The second use of these struts is to allow access from the exterior to the inner hub. A 40 mm diameter hole is taken through the strut so that pipes can be placed inside the hub in order to feed the brake system with oil and to extract the pressurized oil.

Brake system

A hydraulic brake system is used to brake the turbine. This system works with a hydraulic pump that is connected to the rotor disk through its shaft. The oil is pressurized from 1 to 350 bar and, after the oil pressure has been increased, the pressure is decreased down to 1 bar. This pressure dissipation becomes heat that must be removed with an external cooling system that keeps the oil temperature constant. The advantage of this type of system is its simplicity because there is no need to design a bearing system; in the case that an electric generator is used to brake the rotor, it would require a complex electric installation. The hydraulic pump must therefore be calibrated in advance in order to measure the right torque.

Stator and rotor

The purpose of having a turbine stage is to provide realistic boundary conditions at the inlet of the EES section. Therefore, a stator and a rotor turbine are needed. The main turbine parameters are described in Table 3.

The Reynolds number obtained in on design conditions is representative of a compromise between large turbofan engines and geared engines. The aero design of the turbine was done by GKN Aerospace.

The shrouded blades and rotor disk were mechanically analyzed. FEA of static loads on the rotor stage (rotor disk and blades) showed that the rotor blades should be manufactured in aluminium due to the low density of aluminium (compared with steel) and high tensile strength (compared to plastics) and the rotor disk in steel should be manufactured in steel because it has a higher tensile strength than aluminium. A factor of safety of 1.7 was obtained from this analysis. Machined blades are manufactured individually and fastened to the rotor disk using pins. Figure 6b shows a detailed view of this section.

Sealing design

Tip leakage flows influence the flow on the EES creating rolling vortices on the surface of the OGVs and considerably increase the heat transfer rate (see Rojo et al. (2013)) even if the leakage mass flow is around 1% of the total mass flow. The design of the tip sealing is therefore engine like, and the calculated mass flow rate through it is 1±0.3 % due to geometrical tolerances. The tip

Parameter	Value
Re number based on channel height	465,000
Shroud radius [m]	0.553
Hub radius [m]	0.34
Axial velocity [m/s]	32.8
Mass flow rate [kg/s]	22.8
Temperature [K]	300
Flow coefficient (Ca/U)	0.76
Load coefficient ($\Delta H/U^2$)	1.62
Rotor exit flow angle	-35°
Pressure ratio	1.037
Number of NGVs	60
Number of rotor blades	72
Rotational speed [rpm]	920
Torque [N.m]	710
Power [kW]	68.4

Table 3: **Turbine stage parameters for on design conditions.**

sealing design of a rotor blade was done using ANSYS Workbench for geometry parameterization and mesh generation with FLUENT as a solver, which can be used to run 2D axisymmetric simulations including the effects of swirl flow. The first conclusion drawn when this analysis was run is that adding more ribs to the sealing (three ribs case was checked and compared) does not improve the performance of the sealing. Furthermore, it has been found that the flow downstream of the rotor blade does not create a major recirculation at the outlet of the tip sealing.

PRESSURE LOSS CALCULATION

Once the turbine parameters are completely defined, it is possible to start the analysis of the pressure distribution for different reasons. First of all and most important, given the mass flow required to achieve the required speed in the turbine section, it is possible to calculate the pressure distribution along the rig.

To calculate the pressure drop in any section, experimental data obtained from previous rig studies, CFD results on the contraction section and correlations from Barlow et al. (1999) were used. To calculate these correlations, the static pressure was measured at the inlet and outlet of a certain section. The pressure drop correlations for the individual screens were derived based on measurements.

Component	Pressure Drop Coefficient
Second screen	$K = 117.86 \cdot Re^{-0.274}$
Fourth Screen	$K = 785.63 \cdot Re^{-0.339}$
Fifth Screen	$K = 529.59 \cdot Re^{-0.316}$

Table 4: **Experimental correlations for pressure loss calculations obtained from existing HPT rig at Chalmers University of Technology.**

Table 4 summarizes the measured pressure drop coefficients. Figure 7 shows how the correlations obtained a fit with the experimental data and the components that create the highest pressure loss.

Finally, the optimum value for the size of the flow conditioning section obtained for the given

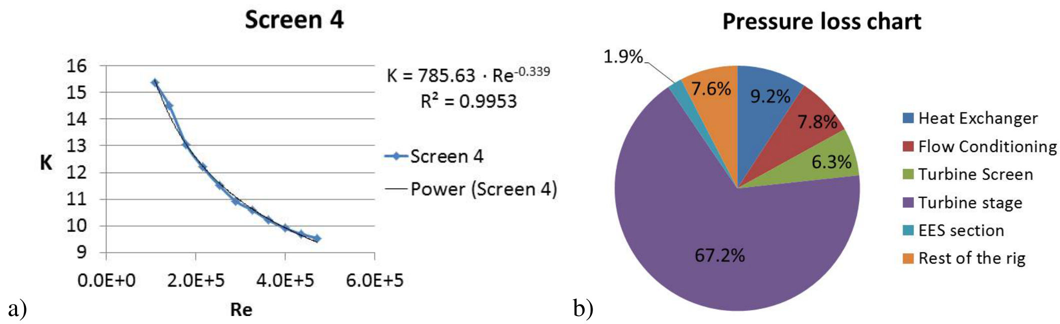

Figure 7: **a) Example of pressure drop coefficient measurement and regression curve. b) Comparison of losses in different sections of the rig .**

turbine design is a diameter of 2 meters; the diffusing section and fan have been designed for these requirements on the basis of this value.

MEASUREMENT TECHNIQUES

Pitot tube, 5-hole probe, 7-hole probe and oil-flow visualization measurement techniques will be used in this rig to make all the measurements listed below. Furthermore, an IR camera will be used to measure surface temperatures on end-walls and vane surfaces. All the experiments that are planned to be performed inside the EES section are listed here.

- Measure steady OGV inlet conditions (total pressure, velocities, angles and turbulence)
- Measure steady LPT inlet conditions (total pressure, velocities, angles and turbulence)
- Measurements on the outlet plane:

  2D plane measurements of total pressure, static pressure, velocities and velocity angles

  Wake profile measurements (total pressure and velocity angles), detailed profiles at a few sections
- End-wall boundary layers, detailed enough to see the end-wall boundary layer sizes.
- Static pressure measurements on vane, end-walls and bumps
- Transition measurements of interest
- Oil-flow visualization on the vane surface and end-walls
- Heat transfer measurements on the end-walls and vane in one sector

CONCLUSIONS

Experimental data obtained from the classical low speed wind tunnel literature and numerical tools have been used in the design of this annular cascade rig. A new method has been developed for the design of axisymmetric contraction ducts with a central body.

In addition, new data and correlations for pressure loss on screens have been obtained. These can be used to obtain an accurate estimation of the pressure loss and therefore enable the possibility to optimize the duct sizes in the rig.

Finally, it is important to point out CFD and empirical correlations have been used in the design of the wind tunnel. CFD results have been especially useful in the design of the sealing and the diffusing section (showing the possibility of having flow separation in the diffuser).

REFERENCES

Abbaspour, M. and Shojaee, M.N., Innovative approach to design a new national low speed wind tunnel, International Journal of Environmental Science and Technology, Vol. 6, No 1, Winter 2009, pp. 23-34.

Arroyo, C., Aerothermal investigation of an intermediate turbine duct, PhD thesis, Chalmers University of Technology, (2009)

Barlow, J.B., Rae, W.H. Jr., and Pope, A., Low-Speed Wind Tunnel Testing, 3rd edition, John Wiley & Sons, Inc., (1999)

Chmielewski G.E., Boundary-Layer Considerations on the Design of Aerodynamic Contractions, Journal of Aircraft, Vol. 11, No. 8 (1974), pp. 435-438

Goldstein, R. J. and Spores, R. A., Turbulent Transport on the Endwall in the Region Between Adjacent Turbine Blades, Transactions of the ASME, Vol. 110 (1988), pp. 862-869

Hjärne, J., Lennart, L. and Larsson, J., Design of a modern test facility for LPT/OGV flows, Vol. 6, No. GT2003-38083 (2003), pp. 137-145

Hjärne, J., Turbine outlet guide vane flows, PhD thesis, Chalmers University of Technology, (2007)

James, H. Bell and Rabindra, D. Mehta, Boundary-layer predictions for small low-speed contractions, AIAA Journal, Vol. 27, Issue 3, March 1989, pp. 372-374

Mikhail, M. N., Optimum Design of Wind Tunnel Contractions, AIAA Journal, Vol. 17, No. 5 (1979), pp. 471-477

Morel, T., Comprehensive Design of Axisymmetric Wind Tunnel Contractions, Journal of Fluids Engineering, Vol. 97, Issue 2 (1975), pp. 225-233

Rojo, B., Johansson, M., Chernoray, V. and Golubev, M., Experimental Heat Transfer Study in an Intermediate Turbine Duct , 49th AIAA Joint Propulsion Conference, AIAA-2013-3622

Rojo, B., Jimenez, C. and Chernoray, V., Experimental Heat Transfer Study of Endwall in a Linear Cascade with IR Thermography, EPJ Web of Conferences, Vol. 67, No. 02100 (2014)

Schönleitner, F., Koch, H., Selic, T., Hoeger, M. and Marn, A., Comparison of the Experimental Results Between a 2D EGV Cascade Test and a Rig Test Under Engine Representative Conditions, Vol. 2C, No. GT2014-26915, pp. 38-53